Circulation

ORIGINAL RESEARCH ARTICLE

Identification of Drug Transporter Genomic Variants and Inhibitors That Protect Against Doxorubicin-Induced Cardiotoxicity

Tarek Magdy, PhD; Mariam Jouni, PhD; Hui-Hsuan Kuo, BS; Carly J. Weddle, BS; Davi Lyra-Leite, PhD; Hananeh Fonoudi, PhD; Marisol Romero-Tejeda, AB; Mennat Gharib, BS; Hoor Javed, BS; Giovanni Fajardo, MD; Colin J.D. Ross, PhD; Bruce C. Carleton, PharmD; Daniel Bernstein, MD; Paul W. Burridge, PhD

BACKGROUND: Multiple pharmacogenomic studies have identified the synonymous genomic variant rs7853758 (G > A, L461L) and the intronic variant rs885004 in *SLC28A3* (solute carrier family 28 member 3) as statistically associated with a lower incidence of anthracycline-induced cardiotoxicity. However, the true causal variant(s), the cardioprotective mechanism of this locus, the role of *SLC28A3* and other solute carrier (SLC) transporters in anthracycline-induced cardiotoxicity, and the suitability of SLC transporters as targets for cardioprotective drugs has not been investigated.

METHODS: Six well-phenotyped, doxorubicin-treated pediatric patients from the original association study cohort were recruited again, and human induced pluripotent stem cell–derived cardiomyocytes were generated. Patient-specific doxorubicin-induced cardiotoxicity (DIC) was then characterized using assays of cell viability, activated caspase 3/7, and doxorubicin uptake. The role of *SLC28A3* in DIC was then queried using overexpression and knockout of *SLC28A3* in isogenic human-induced pluripotent stem cell–derived cardiomyocytes using a CRISPR/Cas9 (Clustered Regularly Interspaced Short Palindromic Repeats/CRISPR-associated protein 9). Fine-mapping of the *SLC28A3* locus was then completed after *SLC28A3* resequencing and an extended in silico haplotype and functional analysis. Genome editing of the potential causal variant was done using cytosine base editor. *SLC28A3-AS1* overexpression was done using a lentiviral plasmid-based transduction and was validated using stranded RNA-sequencing after ribosomal RNA depletion. Drug screening was done using the Prestwick Chemical Library (n = 1200), followed by in vivo validation in mice. The effect of desipramine on doxorubicin cytotoxicity was also investigated in 8 cancer cell lines.

RESULTS: Here, using the most commonly used anthracycline, doxorubicin, we demonstrate that patient-derived cardiomyocytes recapitulate the cardioprotective effect of the *SLC28A3* locus and that SLC28A3 expression influences the severity of DIC. Using Nanopore-based fine-mapping and base editing, we identify a novel cardioprotective single nucleotide polymorphism, rs11140490, in the *SLC28A3* locus; its effect is exerted via regulation of an antisense long noncoding RNA (*SLC28A3-AS1*) that overlaps with *SLC28A3.* Using high-throughput drug screening in patient-derived cardiomyocytes and whole organism validation in mice, we identify the SLC competitive inhibitor desipramine as protective against DIC.

CONCLUSIONS: This work demonstrates the power of the human induced pluripotent stem cell model to take a single nucleotide polymorphism from a statistical association through to drug discovery, providing human cell-tested data for clinical trials to attenuate DIC.

Key Words: cardiotoxicity ■ CRISPR-Cas systems ■ doxorubicin ■ human induced pluripotent stem cells ■ myocytes, cardiac

Editorial, see p 295

Correspondence to: Paul Burridge, PhD, Department of Pharmacology, Northwestern University Feinberg School of Medicine, 320 East Superior Street, Searle Building Suite 8-525, Chicago, IL 60611. Email paul.burridge@northwestern.edu

Supplemental Material is available at https://www.ahajournals.org/doi/suppl/10.1161/circulationaha.121.055801.

For Sources of Funding and Disclosures, see page 292.

Circulation is available at www.ahajournals.org/journal/circ

Clinical Perspective

What Is New?

- This study shows that patient-specific cardiomyocytes recapitulate the cardioprotective effect of the candidate gene association study–identified SLC28A3 (solute carrier family 28 member 3) locus and we functionally confirm for the first time the role of SLC28A3 in doxorubicin-induced cardiotoxicity.
- A novel genetic variant, rs11140490, is the potential causal variant in the SLC28A3 cardioprotective locus.
- The solute carrier transporter inhibitor desipramine protects against doxorubicin-induced cardiotoxicity through decreasing the intracellular uptake of doxorubicin into the heart.

What Are the Clinical Implications?

- We provide 2 potential therapeutic options to attenuate doxorubicin-induced cardiotoxicity: either repurposing US Food and Drug Administration–approved desipramine or therapy with *SLC28A3-AS1* (*SLC28A3* overlapping antisense long noncoding RNA).
- We propose that a simple clinical test to detect the presence of rs11140490 can be used to predict that a patient will be less likely to experience doxorubicin-induced cardiotoxicity and that, with future clinical trials, it may be possible for these patients to be treated with a longer duration (higher cumulative dose) of doxorubicin to enhance the efficacy of their chemotherapy.

Nonstandard Abbreviations and Acronyms

AIC	anthracycline-induced cardiotoxicity
Cas9	CRISPR-associated protein 9
CGAS	candidate gene association study
CRISPR	Clustered Regularly Interspaced Short Palindromic Repeats
DIC	doxorubicin-induced cardiotoxicity
GWAS	genome-wide association study
hiPSC	human induced pluripotent stem cells
hiPSC-CM	human induced pluripotent stem cell–derived cardiomyocyte
ISO	isogenic hiPSC line
SLC	solute carrier
SLC28A3	solute carrier family 28 member 3
SNP	single nucleotide polymorphism

Doxorubicin, a cytotoxic anthracycline antibiotic, is a common anticancer agent used to treat a wide variety of adult and childhood cancers. The cardiotoxicity of anthracyclines has been documented as occurring in 9% of treated adult patients,[1] and on average, it occurs within just 3.5 months after the final chemotherapy dose; 98% of patients experience cardiotoxicity within the first year.[1] Early cardiotoxicity leads to dose limitation or treatment discontinuation to the detriment of therapy. The cardiotoxicity of doxorubicin is also well understood to be dose dependent, with 65% and 85% of cancer patients experiencing a decline in left ventricular ejection fraction when treated with 550 and 700 mg/m^2 of doxorubicin, respectively.[2] However, despite attempts to severely limit cumulative dose, cardiotoxicity occurs in 14.5% of patients with breast cancer receiving the most common 240-mg/m^2 cumulative dose.[3]

Pharmacogenomic research has attempted to discover predictive DNA biomarkers for anthracycline-induced cardiotoxicity (AIC) and has so far identified about 75 AIC-associated loci.[4,5] However, the true connection between these loci and cardiotoxicity is unknown, given that the majority of AIC pharmacogenomic studies lack functional validation of the identified associations. As a result, no US Food and Drug Administration–approved genetic biomarkers are currently being used in routine clinical practice that predict AIC,[6] and only a single on-market drug, dexrazoxane, is approved to decrease the incidence of AIC.

SLC28A3 encodes solute carrier (SLC) transporter family 28 member 3 and is the most robustly replicated AIC-associated cardioprotective loci. This locus was initially discovered in a large, multicenter pediatric candidate gene association study (CGAS) that identified 2 single nucleotide polymorphisms (SNPs): rs7853758 (G > A, L461L), which is in a coding region but synonymous, and rs885004, which is located in intron 8. Both SNPs are in high linkage disequilibrium. rs7853758 is highly associated with a lower risk of developing doxorubicin-induced cardiotoxicity (DIC) in both discovery (n = 188; $P^{adj} = 0.0071$; odds ratio [OR] = 0.29) and replication (n = 156; $P^{adj} = 0.0072$; OR = 0.33) cohorts.[7] It is important to note that this genetic association was replicated in a third additional multicenter independent cohort of 218 patients.[8] The sensitivity and specificity (95% CI) of rs7853758 is 17.4 (7.8–31.4) and 64.6 (58.8–70.1), respectively.[9] Despite identification of this SNP through 2 replication cohorts in CGAS, the mechanisms by which a synonymous variant can influence AIC is unclear. Thus, the validity of this locus in relation to AIC, the true causal variant and the cardioprotective mechanism of this locus, the role of SLC28A3 and other SLC transporters in AIC, and the suitability of SLC transporters as targets for cardioprotective drugs are critical uninvesitgated topics.

Here, we show that patient-specific human induced pluripotent stem cell (hiPSC)–derived cardiomyocytes (hiPSC-CMs) recapitulate the cardioprotective effect of SNP rs7853758. *SLC28A3* knockdown and overexpression using CRISPR/Cas9 (Clustered Regularly Interspaced Short Palindromic Repeats/CRISPR-associated protein 9) reduces and increases doxorubicin uptake

into cardiomyocytes, respectively, altering their sensitivity to doxorubicin, thus confirming the role of this locus in DIC. Fine-mapping of the *SLC28A3* locus uncovered that rather than the original CGAS-identified synonymous SNP (rs7853758), the linked SNP rs11140490 is the causal cardioprotective variant in that locus. Further mechanistic studies showed that rs11140490 exerts its action by regulating an *SLC28A3*-overlapping, antisense long noncoding RNA *SLC28A3-AS1*. Screening for other potential cardiac-specific SLC transporters in relation to DIC revealed that *SLC22A4* and *SLC22A17* are also implicated in DIC. Last, screening a drug library using hiPSC-CMs followed by in vivo validation in a mouse model of DIC discovered that the SLC competitive inhibitor, desipramine protects against DIC by without hindering doxorubicin chemotherapy efficacy. Together, these findings provide a novel genetic test for rs11140490 that can identify patients who are protected from DIC and 2 potential therapeutic options, either using the long noncoding RNA *SLC28A3-AS1* or developing a derivative of desipramine to attenuate DIC.

METHODS

The data, analytic methods, and study materials are available to other researchers on reasonable request for purposes of reproducing the results. Detailed methods are provided in the Supplemental Material. RNA-sequencing data have been deposited in Gene Expression Omnibus (https://www.ncbi.nlm.nih.gov/geo/) with accession code GSE165731.

Human Induced Pluripotent Cell Derivation and Cardiac Differentiation

Protocols and consents were approved by the institutional review boards of Northwestern University and University of British Columbia. Six well-phenotyped, doxorubicin-treated pediatric patients from the original association study cohort were recruited again with informed consent. Peripheral blood mononuclear cells were isolated from blood and reprogramed to hiPSCs using CytoTune–iPS 2.0 Sendai Reprogramming Kit (Invitrogen).[10] SNP karyotyping was performed using a whole-genome Infinium HumanCytoSNP–12 BeadChip Array (Illumina). Differentiation into cardiomyocytes was performed according to previously described protocol with some modifications[11,12] including the use of a *TNNT2* (cardiac troponin T)–driven antibiotic selection cassette for cardiomyocyte purification.

CRISPR/Cas9–Mediated Gene Knockout and Overexpression

To generate *SLC28A3* knockout gRNA expression vectors, gRNA targeting the start codon designed with minimal predicted off-target effect.[13] Each gRNA was annealed and inserted into pSpCas9(BB)-2A-Puro (PX459) V2.0 (48138; Addgene) plasmid that expresses puromycin resistance gene for downstream antibiotic selection, in addition to Cas9. One million cells were electroporated with 5 µg PX459 plasmid and positive clones were selected 24 hours after transfection using puromycin treatment for 48 hours. To generate *SLC28A3* overexpressing cells, Human *SLC28A3* Sequence-Verified cDNA was first amplified and cloned under the CAG promoter of a pAAVS1–Nst–CAG–DEST gateway cloning vector (80489; Addgene). *AAVS1* (adeno-associated virus integration site 1) gRNA expression vector[14] (pXAT2; 80494, Addgene), which expresses gRNA and Cas9, was used to target *AAVS1* locus in the first intron of the *PPP1R12C* (protein phosphate 1 regulatory subunit 12C) gene.[14] Cells were then electroporated with AAVS1 targeting plasmid and SLC28A3 overexpression donor plasmid. Positive clones were selected using neomycin treatment for 14 days.

Patient-Specific DIC Characterization

Patient-specific DIC was characterized by assays of cell viability using CellTiter–Glo 2.0 (Promega) and activated caspase 3/7 using Caspase 3/7–Glo (Promega) that were used per manufacturer's instructions. Doxorubicin uptake was quantified using flow cytometry by measuring doxorubicin intrinsic phycoerythrin fluoroscence at 1 and 3 hours after doxorubicin treatment and normalized to baseline fluorescence. All cells were stained with NucRed Live ReadyProbes Reagent (Invitrogen) to monitor cell viability.

SLC28A3 Locus Genetic Fine-Mapping

Fine-mapping of the *SLC28A3* locus was then completed after *SLC28A3* resequencing using MinION Nanopore sequencer and an extended in silico haplotype and functional analysis.

Genome Editing of Potential Causal Variant rs11140490

Locus-specific base-editor protein complex and gRNA were designed using Beditor,[15] and the designed gRNA was cloned in the gRNA expressing plasmid (73797; Addgene). Then, 1 million cells were electroporated with 4 µg of the base editor–expressing plasmid (119861; pSI-Target-AID-NG; Addgene) and 4 µg of the gRNA-expressing plasmid (73797; lenti sgRNA[MS2]_puro; Addgene). Cells were then selected with puromycin 24 hours after transfection for 48 hours, clones were hand-picked, the target locus was polymerase chain reaction–amplified and Sanger sequenced to confirm the SNP editing in all clones.

SLC28A3-AS1 Overexpression in Isogenic hiPSCs

The *SLC28A3-AS1* cDNA was cloned into pLenti-C-Myc-DDK-IRES-Puro lentiviral vector (OriGene), which was then cotransfected with packaging plasmids psPAX2 (12260; Addgene) and pMD2.G (12259; Addgene) into Lenti-X 293T cells (Takara) to generate lentivirus. Virus-containing supernatant was collected at 48 and 72 hours posttransfection. Lentivirus was concentrated 1:100 from cleared supernatant using PEG-it (Systems Biosciences). Isogeneic hiPSCs were then transduced and positive clones were selected with puromycin for 7 days to generate $ISO^{SLC28A3\text{-}AS1}$. *SLC28A3-AS1* overexpression was confirmed using stranded RNA-sequencing after ribosomal RNA depletion.

Mouse Model of Doxorubicin-Induced Cardiomyopathy and Drug Administration

Procedures were followed in accordance with Stanford University's institutional guidelines. In vivo validation was done using 10-week-old male C57BL/6J mice that were cotreated with doxorubicin (NovaPlus) and water as a control vehicle (n = 10), or with desipramine (Sigma) in the experimental groups (n = 8). At day 0, mice were treated with doxorubicin (3 mg/kg) intraperitoneally twice a week alone or with desipramine by Alzet pump infusion (20 $mg{\cdot}kg^{-1}{\cdot}day^{-1}$) for 3 weeks (days 0–21). For the control group, we treated mice with corn oil on the same schedule as desipramine administration. We recorded an echocardiogram once a week (on days 0, 7, 14, and 21) and terminated the experiment at day 21.

Statistical Analysis

Data were analyzed in R version 4.0.3 and graphed in GraphPad Prism 6. Detailed statistical information is included in the corresponding figure legends. Data were presented as mean±SEM. Comparisons were conducted using a 1-way ANOVA test or an unpaired 2-tailed Student *t* test with significant differences defined as $P<0.05$ (*), $P<0.01$ (**), $P<0.001$ (***), and $P<0.0001$ (****). Our sample size (3 patients in each category) was based on the feasibility of handling this number of hiPSC lines. For dose–response curves, a log-logistic nonlinear regression model was used to estimate the value of the 4 parameters, and a *t* statistic was used to test for significant difference in LD_{50} between groups using the drc package[16] in R.

RESULTS

Investigation of the Protective Role of Variant rs7853758

Six well-phenotyped, doxorubicin-treated pediatric patients from the original CGAS cohort were specifically recruited again according to the original inclusion criteria[17] (Table S1). These included 3 patients who were heterozygous for the rs7853758 variant and were protected from DIC (SLC^{var1}, SLC^{var2}, SLC^{var3}; collectively SLC^{var}), and 3 control patients who did not carry this protective variant (they carry the reference allele) and developed DIC after the doxorubicin therapy (SLC^{ref1}, SLC^{ref2}, SLC^{ref3}; collectively SLC^{ref}). Detailed patient data including age, sex, ethnicity, type of cancer, treatment regimen, and presence or absence of DIC are provided in Table S2. hiPSC lines were established from peripheral blood of patients using nonintegrating (Sendai virus–based) reprogramming and our well-established protocols.[18,19] These lines showed normal hiPSC morphology (Figure S1A), expressed high levels of undifferentiated cell markers (Figure S1B and S1C), and were karyotypically normal (Figure S2). The genotypes of the rs7853758 SNP were validated using Nanopore-based sequencing (Figure 1A). Cardiomyocytes were generated using our established chemically-defined, small molecule–based monolayer differentiation system[11,20] (Figure S3A), along with a TNNT2-based antibiotic selection cassette that consistently produces cardiomyocytes that are 80% to 98% $TNNT2^{+}$ (Figure S3B and S3D). hiPSC-CMs express *SLC28A3* throughout the cell (Figure 1B).

Patient-Specific hiPSC-CMs Recapitulate the Cardioprotective Effect of rs7853758 Against DIC

We first aimed to model the cardioprotective effect of rs7853758 variant in patient–specific hiPSC-CMs. A cell viability assay completed at 72 hours after doxorubicin treatment demonstrated that the 3 SLC^{var} lines recapitulated the protective effect of SNP ([rs7853758 G > A; L461L] $LD_{50} = 2.7$ μmol/L; $P<0.0001$; n = 126) as compared with the SLC^{ref} lines ($LD_{50} = 1.38$ μmol/L; n = 81) (Figure 1C; Figure S12A). Consistently, apoptosis as quantified by a caspase-3 and -7 activity assay completed 72 hours after doxorubicin treatment was significantly lower in SLC^{var} lines ($IC_{50} = 1$ μmol/L; $P=0.001$; n = 20) compared with the SLC^{ref} lines ($IC_{50} = 0.43$ μmol/L; n = 20; Figure 1D). Because *SLC28A3* is an uptake transporter, we hypothesized that the lower level of DIC in the SLC^{var} lines might be attributable to reduced doxorubicin uptake as a result of impaired *SLC28A3* function in these patients. To test this, we used a flow cytometry–based assay and found that intracellular doxorubicin uptake was ≈50% lower in SLC^{var} as compared with SLC^{ref} (Figure 1E), which is consistent with the magnitude LD_{50} (1.38 μmol/L versus 2.7 μmol/L) and IC_{50} (0.43 μmol/L versus 1 μmol/L) changes on our in vitro DIC assays (Figure 1C). To investigate whether this cardioprotective effect seen in SLC^{var} is attributable to altered SLC28A3 protein expression, we then quantified SLC28A3 in our patient-specific hiPSC-CMs using Western blot. SLC28A3 expression in SLC^{var} was significantly lower than SLC^{ref} ($P = 0.03$) (Figure S1F; Figure S12B).

SLC28A3 Altered Expression Affects DIC in hiPSC-CMs

To further confirm the implication of *SLC28A3* in DIC regardless of patient-specific genetic, transcriptomic, and environmental background, and to isolate the effect of *SLC28A3* in relation to DIC, we next examined whether a gain or loss of function of *SLC28A3* altered DIC in an isogenic hiPSC line (ISO). The ISO line was derived from a healthy individual and its whole genome sequencing confirmed that it does not harbor any other DIC-associated loci identified by the original study. *SLC28A3* overexpression and knockout (KO) lines were generated through a CRISPR/Cas9–mediated approach. Disturbance at start codon region was confirmed by Sanger sequencing (Figure 2A and 2B) and altered *SLC28A3* expression in these lines was confirmed by quantitative reverse transcription poly-

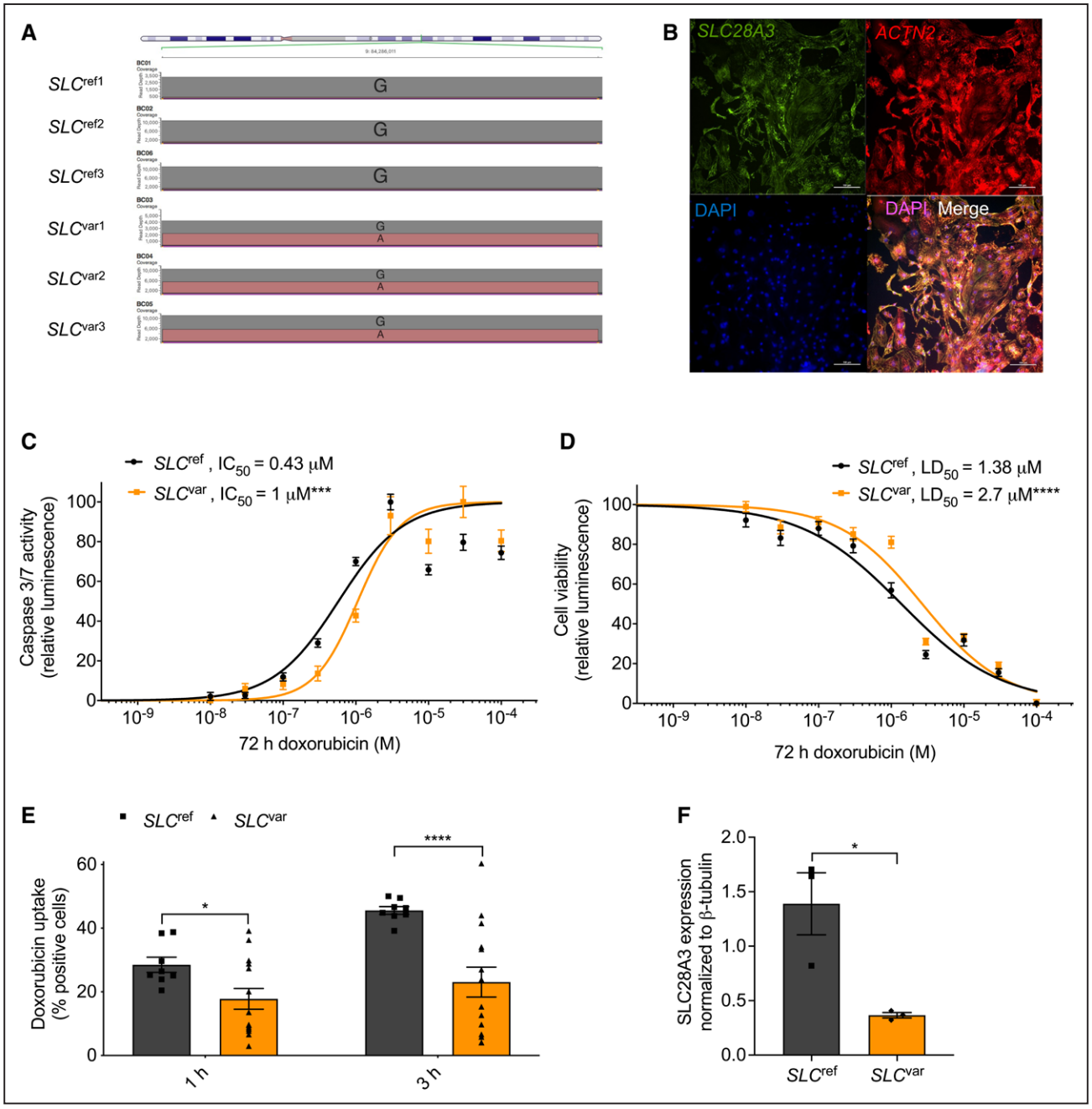

Figure 1. Patient-specific human induced pluripotent stem cell–derived cardiomyocytes (hiPSC-CMs) recapitulate the cardioprotective effect of *SLC28A3* variant rs7853758.

Comparison of hiPSC-CMs derived from 3 patients who harbor the heterozygous rs7853758 variant and were protected from DIC after doxorubicin treatment (*SLC*^{var1}, *SLC*^{var2}, *SLC*^{var3}; collectively, *SLC*^{var}) to hiPSC-CMs from 3 control patients who did not carry this protective SNP and developed doxorubicin-induced cardiotoxicity on the same doxorubicin treatment (*SLC*^{ref1}, *SLC*^{ref2}, *SLC*^{ref3} *SLC*^{ref3}*SLC*^{ref3}; collectively, *SLC*^{ref}). **A**, Nanopore sequencing reads at SNP rs7853758 locus, confirming its genotypes in all patient-derived hiPSC lines. **B**, Immunofluorescent staining showing the expression and localization of *SLC28A3* throughout the cell in patient-derived hiPSC-CMs. **C**, Effect of doxorubicin (72 h) on cell viability in *SLC*^{var} (n = 126) and *SLC*^{ref} (n = 81) hiPSC-CMs measured by a CellTiter-Glo 2.0 assay. **D**, Effect of doxorubicin (72 h) on apoptosis measured by activated caspase 3/7 in *SLC*^{var} (n = 20) and *SLC*^{ref} (n = 20) hiPSC-CMs. **E**, Assessment of doxorubicin uptake through measurement of percentage of cells with doxorubicin intrinsic fluorescence using a flow cytometry–based assay in patient-derived hiPSC-CMs (n = 8–13). **F**, SLC28A3 expression in *SLC*^{ref} (n = 3) and *SLC*^{var} (n = 3) hiPSC-CMs using Western blot. **C** and **D**, Log-logistic nonlinear regression model was used to estimate the value of the 4 parameters, and a t-statistic was used to test for significant difference in LD_{50} between groups. N = full independent experimental replicates. Error bars indicate SEM; $^{*}P \le 0.05$, $^{**}P \le 0.01$, $^{***}P \le 0.001$, $^{****}P \le 0.0001$ by unpaired 2-tailed Student *t* test (**E** and **F**). SEM indicates standard error of the mean; and SLC28A3, solute carrier family 28 member 3.

merase chain reaction and Western blot showing 90% downregulation of SLC28A3 in ISO-KO (Figure 2C). The effect of *SLC28A3* overexpression and KO on in vitro DIC was investigated using the above cell viability and caspase assays at 72 hours after doxorubicin treatment. The cell viability assay showed that the ISO

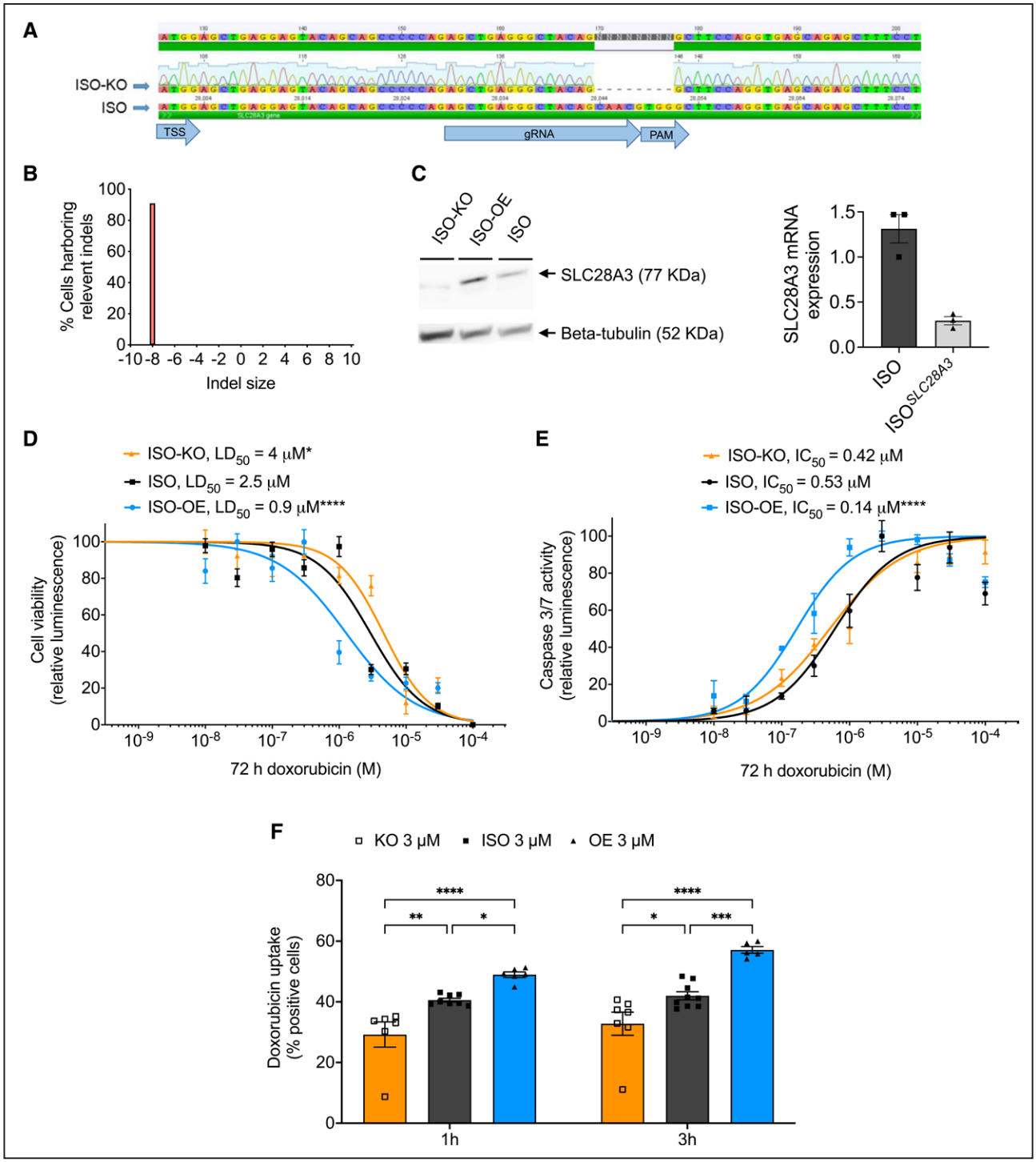

Figure 2. SLC28A3 expression affects the severity of doxorubicin-induced cardiotoxicity by regulating doxorubicin uptake into cardiomyocytes.

A, Validation of CRISPR/Cas9–mediated *SLC28A3* KO in an isogenic human induced pluripotent stem-cell line detected by Sanger sequencing, showing 8-bp deletion downstream of the TSS. **B**, Demonstration that 91% of the cell population acquire the introduced deletion. **C**, Validation of KO and AAVS1-based *SLC28A3* OE by Western blot and reverse transcription polymerase chain reaction. **D**, Effect of doxorubicin (72 h) on viability in ISO (n = 45), ISO-OE (n = 14), and ISO-KO (n = 6) human induced pluripotent stem cell–derived cardiomyocytes. **E**, Effect of doxorubicin (72 h) on apoptosis measured by activated caspase 3/7 in ISO (n = 8), ISO-OE (n = 10), and ISO-KO (n = 6) human induced pluripotent stem-cell cardiomyocytes. **F**, Assessment of doxorubicin uptake through measurement of doxorubicin intrinsic fluorescence using flow cytometry–based assay (n = 6–9). **D** and **E**, A log-logistic nonlinear regression model was used to estimate the value of the 4 parameters, and a t-statistic was used to test for significant difference in LD_{50} between groups. N = full independent experimental replicates. Error bars indicate SEM. $^{*}P \le 0.05$, $^{**}P \le 0.01$, $^{***}P \le 0.001$, $^{****}P \le 0.0001$ by unpaired 2-tailed Student *t* test (**F**). ISO indicates isogenic hiPSC line; KO, knockout; OE, overexpression; PAM, protospacer adjacent motif; SEM, standard error of the mean; SLC28A3, solute carrier family 28 member 3; and TSS, transcription start site.

overexpression hiPSC-CMs (LD_{50} = 0.9 µmol/L) were ≈3.3-fold and 1.4-fold more sensitive to doxorubicin as compared with ISO-KO (LD_{50} = 4 µmol/L; P=0.03) and ISO (LD_{50} = 2.5 µmol/L; P<0.0001), respectively (Figure 2D). Likewise, caspase activity was ≈2.6-fold higher in ISO overexpression (LD_{50} = 0.14 µmol/L) as compared with ISO (LD_{50} = 0.53 µmol/L, P<0.0001) (Figure 2E). We next aimed to investigate the effect of *SLC28A3* KO and overexpression on doxorubicin intracellular uptake. Doxorubicin uptake was significantly higher in ISO overexpression as compared with ISO both at 1 hour (P=0.035) and 3 hours (P<0.0017) after doxorubicin treatment (Figure 2F). Similarly, doxorubicin uptake was significantly lower in ISO-KO as compared with ISO both at 1 hour (P=0.0009) and 3 hours (P=0.0006) after doxorubicin treatment (Figure 2F). These findings show that *SLC28A3* is implicated in DIC regulation through affecting doxorubicin uptake into cardiomyocytes.

Fine-Mapping at the *SLC28A3* Locus Prioritizes Potential Causal Variant

rs7853758 is a coding synonymous SNP located in exon 14 and thus does not affect the amino acid sequence. Because of the tag SNP and linkage disequilibrium issues associated with GWAS,[21] we expected that rs7853758 is linked (coinherited) to additional SNPs including the causal one(s). To elucidate this, we next fine-mapped the *SLC28A3* locus to identify the potential causal variant. We sequenced the *SLC28A3* gene in all 6 SLC^{var} and SLC^{ref} patients using a Nanopore MinION sequencer and SNPs were called using Nanopolish[22] (see Supplemental Methods). For all patients, Nanopore genotypes of the original association study hit, rs7853758 were in concordance with the GWAS chip genotypes (Figure 1A). In total, 133 SNPs were identified, all of which have at least 1 variant allele in at least 1 patient (Figure S4E). The vast majority of identified SNPs were intronic (n = 93), 25 SNPs were located in 5'-UTR (untranslated region), 12 SNPs were located in 3'-UTR, in addition to 3 coding SNPs of which 2 were synonymous and 1 nonsynonymous (Table S6). We then examined which SNPs were exclusively coinherited in cardioprotected patients and identified a cardioprotective haplotype, $Hap^{SLC28A3}$ comprising 24 SNPs that is coinherited only in cardioprotected patients. These SNPs are distributed as follows, 8 SNPs are located in the 3'-UTR, 14 SNPs are intronic, and 2 are coding synonymous SNPs (Figures 3A–3B; Table S6).

It is interesting that 7 SNPs within $Hap^{SLC28A3}$ are located within a long noncoding RNA (ensemble gene id: ENSG00000233262) that we called "*SLC28A3-AS1*" (submitted to HUGO Gene Nomenclature Committee registry) that overlaps with *SLC28A3* forming another haplotype, $Hap^{SLC28A3\text{-}AS1}$ (Figure 3A; Figures S5A–B). $Hap^{SLC28A3\text{-}AS1}$ consists of SNPs, rs11140490 (A>G), rs10868135 (T > C), rs4877831 (C > G), rs4877833 (T>C), rs7853066 (A>G), rs7853758 (G>A), and rs7030019 (A>G).

To validate and confirm the linkage disequilibrium pattern of the Nanopore-identified cardioprotective haplotype, $Hap^{SLC28A3}$, we investigated the haplotype structure and allelic frequency of this cardioprotective haplotype on a wider population level in 99 individuals of the CEU population, the same ethnic population of the study cohort. This analysis showed that the 24 SNPs constituting the $Hap^{SLC28A3}$ were in high linkage disequilibrium with an average D' and R^2 of 0.99 and 0.84, respectively (Figure S5A and S5B; Table S11). Regarding $Hap^{SLC28A3\text{-}AS1}$, 7 structures were identified, Hap-$I^{SLC28A3\text{-}AS1}$ to Hap-$VII^{SLC28A3\text{-}AS1}$ (Figure S5C). In that, Hap-$I^{SLC28A3\text{-}AS1}$ consists of the reference alleles for all 7 SNPs (ATCTAGA) and is inherited in 71.7% of the examined population, whereas Hap-$II^{SLC28A3\text{-}AS1}$ comprises the variant alleles for all 7 SNPs (GCGCGAG) and is inherited in 17.7% of the examined population (Figure S5C). This finding confirms the linkage disequilibrium pattern identified by the Nanopore pipeline in all of the study patients.

To eliminate the probability that the causal variant might be located in one of the adjacent genes to the *SLC28A3/SLC28A3-AS1* target locus, we did an extended linkage disequilibrium analysis to include all variants that are located with 1 MB up and downstream of the target locus in both European (the same ethnic population of the original genotype–phenotype association study) and all ethnicity populations. These analyses did not identify any other SNPs that are linked to rs7853758 and are not included in our original haplotype analysis. This eliminates the probability that the causal cardioprotective variant is located in adjacent genes (Figure S6).

To prioritize cardioprotective haplotype SNPs, we investigated the regulatory properties of all candidate SNPs (n = 24). Using ENCODE (Encyclopedia of DNA Elements) and Roadmap Epigenomics[23] data, and DeepSEA[24] algorithm, we examined the functional effect of each SNP on altering chromatin features (transcription factors, Dnase hypersensitive site, and histone marks) binding sites. Among all SNPs, rs11140490 and rs4877835 had the top chromatin regulatory effect as both SNPs predicted to alter the binding site of 206 and 204 chromatin features, respectively (Figure S4F; Tables S7–S8). Moreover, SNP rs11140490 has the most substantial regulatory effect as it is predicted to alter the binding sites of 43 features with $\log_2$ fold change of ≥1, whereas rs4877835 is predicted to alter the binding sites of only 4 features with $\log_2$ fold change of ≥1. It is unsurprising that the primary study significant association, rs7853758 does not show any significant chromatin regulatory effect (Figure 4G).

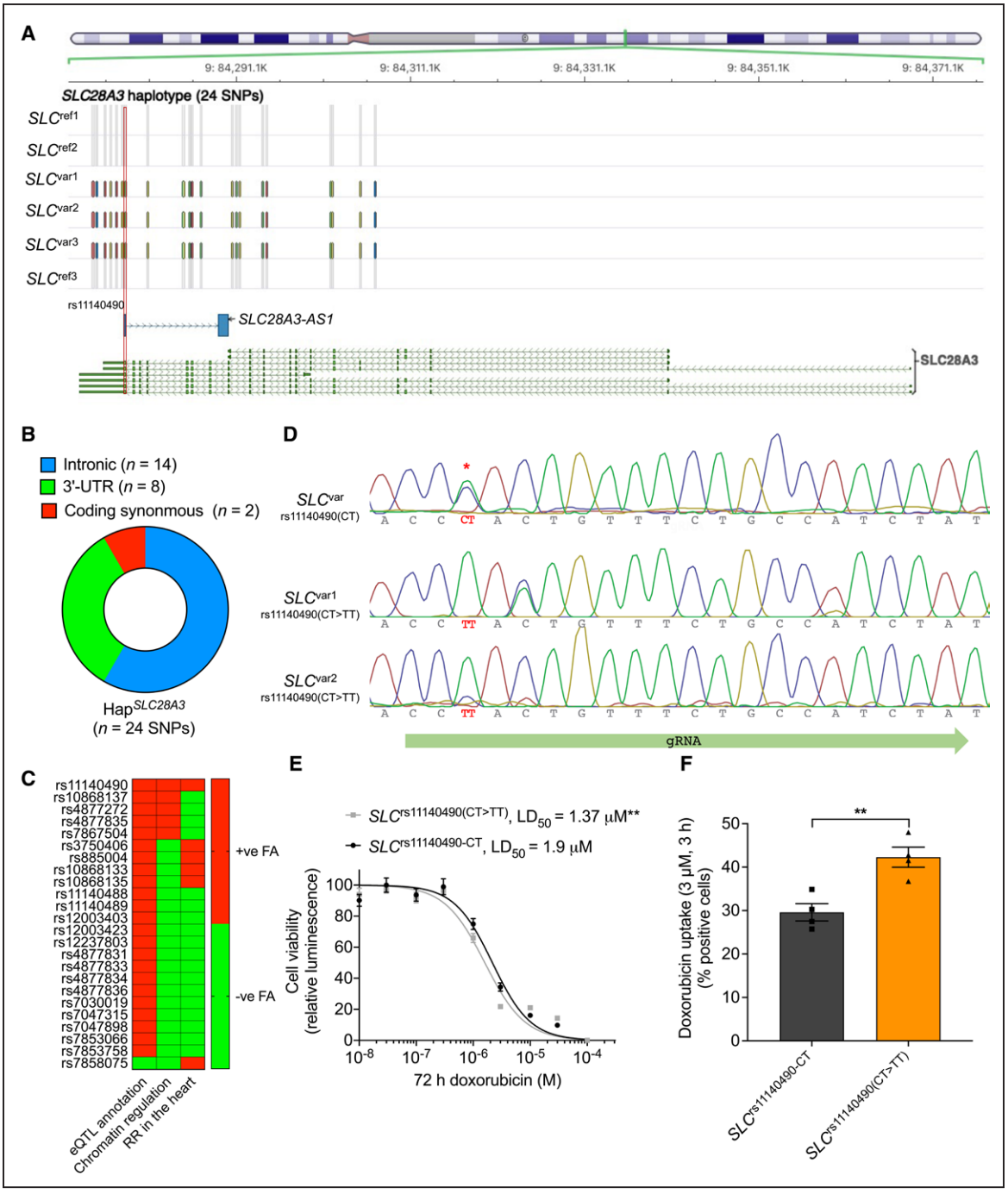

Figure 3. Fine-mapping at the *SLC28A3-SLC28A3-AS1* locus identifies rs11140490 as the potential causal cardioprotective variant. **A**, Location of the Hap^{SLC28A3} comprising 24 SNPs that are coinherited only in *SLC*^{var}-protected patients. SNP rs11140490 marked by red rectangle is located at the splice site of the first exon of an overlapping long noncoding RNA, *SLC28A3-AS1* (adapted from Magdy et al[29]). **B**, Consequence of coinherited Hap^{SLC28A3} SNPs (n = 24). **C**, Overall prioritization of candidate causal SNPs based on functional annotation analyses including, expression quantitative trait loci annotation, chromatin regulatory analyses, and overlapping with RR in cardiac tissues. **D**, Editing of rs11140490 (CT > TT) in 2 patient-specific human induced pluripotent stem cell lines using a cytosine base editor (Target-AID-NG); rs11140490 is indicated by the red asterisk. **E**, Effect of doxorubicin (72 h) on viability in *SLC*$^{var\text{-}rs11140490\ (CT)}$ (2 lines; n = 31) and *SLC*$^{var\text{-}rs11140490(CT>TT\ edited)}$ (2 lines; n = *75*) human induced pluripotent stem cell–derived cardiomyocytes. **F**, Assessment of doxorubicin uptake through measurement percentage of cells with doxorubicin intrinsic fluorescence using flow cytometry–based assay in *SLC*$^{var\text{-}rs11140490\ (CT)}$ and *SLC*$^{var\text{-}rs11140490(CT>TT\ edited)}$ (n = 4). **E**, Log-logistic nonlinear regression model was used to estimate the value of the 4 parameters, and t-statistic was used to test for significant difference in LD_{50} between groups. N = full independent experimental replicates. Error bars indicate SEM, $^{*}P \le 0.05$, $^{**}P \le 0.01$, $^{***}P \le 0.001$, $^{****}P \le 0.0001$ by unpaired 2-tailed Student *t* test (**F**). eQTL indicates expression quantitative trait loci; FA, functional annotation (adapted from Magdy et al[29]); RR, regulatory regions; SEM, standard error of the mean; SLC28A3, solute carrier family 28 member 3; *SLC28A3-AS1*, *SLC28A3* overlapping antisense long noncoding RNA; and SNP, single nucleotide polymorphisms.

Because DIC affects cardiomyocytes, we performed an additional regulatory analysis exclusively focusing on human cardiac tissue, and for that we used ensemble regulatory build that includes transcription factors, histone mark, and Dnase hypersensitive regions. Six SNPs, rs11140490, rs4877835, rs4877831, rs7047898, rs885004, and rs10868137 were found to be located in at least 1 regulatory region in human cardiac tissue (Table S9). Last, to investigate further regulatory consequences of these candidate SNPs, we used the Genotype-Tissue Expression project database (https://www.gtexportal.org/home/) to investigate which of the identified candidate SNPs have been shown to be an expression quantitative trait loci. All candidate SNPs except rs7858075 have been previously identified as expression quantitative trait loci in cultured fibroblasts, thyroid, and brain tissues (Table S10). Although the expression quantitative trait loci identified by the Genotype-Tissue Expression database are located in noncardiac tissues, these associations emphasize the regulatory function of these SNPs. These findings, when taken together, suggest that SNP rs11140490, located at the splice site of the first exon of *SLC28A3-AS1*, is the SNP with the highest likelihood to be the causal cardioprotective SNP (Figure 3C).

Editing hiPSC-CM rs11140490 Confirms Causality in Relation to Protection Against DIC

After we prioritized rs11140490 to be the top candidate causal variant within the DIC-associated *SLC28A3–SLC28A3-AS1* locus, we confirmed the causality of this variant. Using a base editor–mediated approach, we edited the SNP rs11140490 in hiPSCs from 2 SLC^{var} patients that harbor the heterozygous genotype CT back to the reference genotype TT. The cytosine base editor that we have used is composed of a catalytically inactive "dead" Cas9 fused to cytosine base editor cytidine deaminase that converts a CG base pair to a TA base pair. It is important to note that the cytosine base editor does not induce a DNA cut and thus helped us avoid the mono-allelic genomic deletions and loss-of-heterozygosity problem associated with the homology directed repair (HDR)–based genomic editing approaches.[25] Positive hiPSC clones were differentiated into cardiomyocytes, and DIC and doxorubicin uptake were quantified using the aforementioned assays. $SLC^{rs11140490(CT>TT)}$ cardiomyocytes were more sensitive to doxorubicin (LD_{50} = 1.37 μmol/L; P=0.005) as compared with $SLC^{rs11140490(CT)}$ (LD_{50} = 1.9 μmol/L; Figure 3E). Moreover, doxorubicin uptake was significantly higher in $SLC^{rs11140490(CT>TT)}$ when compared with $SLC^{rs11140490(CT)}$ at 3 hours after doxorubicin treatment (P=0.006; Figure 3F). This finding confirms that the SNP rs11140490 is the causal cardioprotective SNP affecting DIC.

Variant rs11140490 Exerts Cardioprotective Effect by Regulating Long Noncoding RNA *SLC28A3-AS1*

Next, we investigated the cardioprotective mechanism of rs11140490. This variant is located at the splice site of the first exon of the antisense *SLC28A3-AS1* that overlaps with *SLC28A3*. Thus, we hypothesized that SNP rs11140490 might exert its cardioprotective action through regulating the transcription of *SLC28A3-AS1*, which in turn alters the expression of doxorubicin-related genes including *SLC28A3*, and eventually alters the susceptibility of patients to DIC. To test this hypothesis, we investigated the effect of altered expression of *SLC28A3-AS1* on DIC phenotype. We overexpressed *SLC28A3-AS1* in an isogenic cell line ($ISO^{SLC28A3\text{-}AS1}$) by transducing isogenic hiPSCs with the *SLC28A3-AS1* cDNA cloned into pLenti-*MYC*-DDK-IRES-Puro lentivirus expression vector (PS100069; OriGene). *SLC28A3-AS1* overexpression was confirmed by stranded RNA-sequencing after ribosomal RNA depletion (Figure 4A). We then assessed the effect *SLC28A3-AS1* overexpression on *SLC28A3* expression in cardiomyocytes and showed that *SLC28A3* is significantly downregulated in $ISO^{SLC28A3\text{-}AS1}$ cardiomyocytes after doxorubicin treatment (Figure 4B). We then investigated the effect of *SLC28A3-AS1* overexpression on DIC and doxorubicin uptake as before. $ISO^{SLC28A3\text{-}AS1}$ hiPSC-CMs were significantly more resistant to doxorubicin (LD_{50} = 8.4 μmol/L; P<0.0001) as compared with ISO (LD_{50} = 1.8 μmol/L; Figure 4C). Moreover, doxorubicin uptake was significantly impaired in $ISO^{SLC28A3\text{-}AS1}$ cardiomyocytes when compared with ISO at both 1 hour (P = 0.001) and 3 hours (P < 0.001) after doxorubicin treatment (Figure 4D). These results show that the regulation of *SLC28A3-AS1* is a potential mechanism by which SNP rs11140490 exerts its cardioprotective effect.

Implication of Other *SLC* Transporters on DIC Regulation

After we provided proof of principle for the importance of SLC transporters in DIC by showing that *SLC28A3* expression and genomic variants affect the severity of DIC, we examined other potential SLC transporters that might affect DIC. To date, there are more than 450 identified SLC transporters, 12 of which have been shown to either transport doxorubicin or a doxorubicin metabolite and/or their genes harbor SNPs that are significantly associated with doxorubicin clinical outcomes.[26] We examined which of these 12 *SLC* transporters are expressed in adult heart tissue, fetal heart tissue, and hiPSC-CMs. Only 3 additional SLC transporters met these criteria; *SLC22A4*, *SLC22A3*, and *SLC22A17* were selected for further investigation (Figure 4E). For each of these transporters, we generated CRISPR/Cas9–mediated KO hiPSC

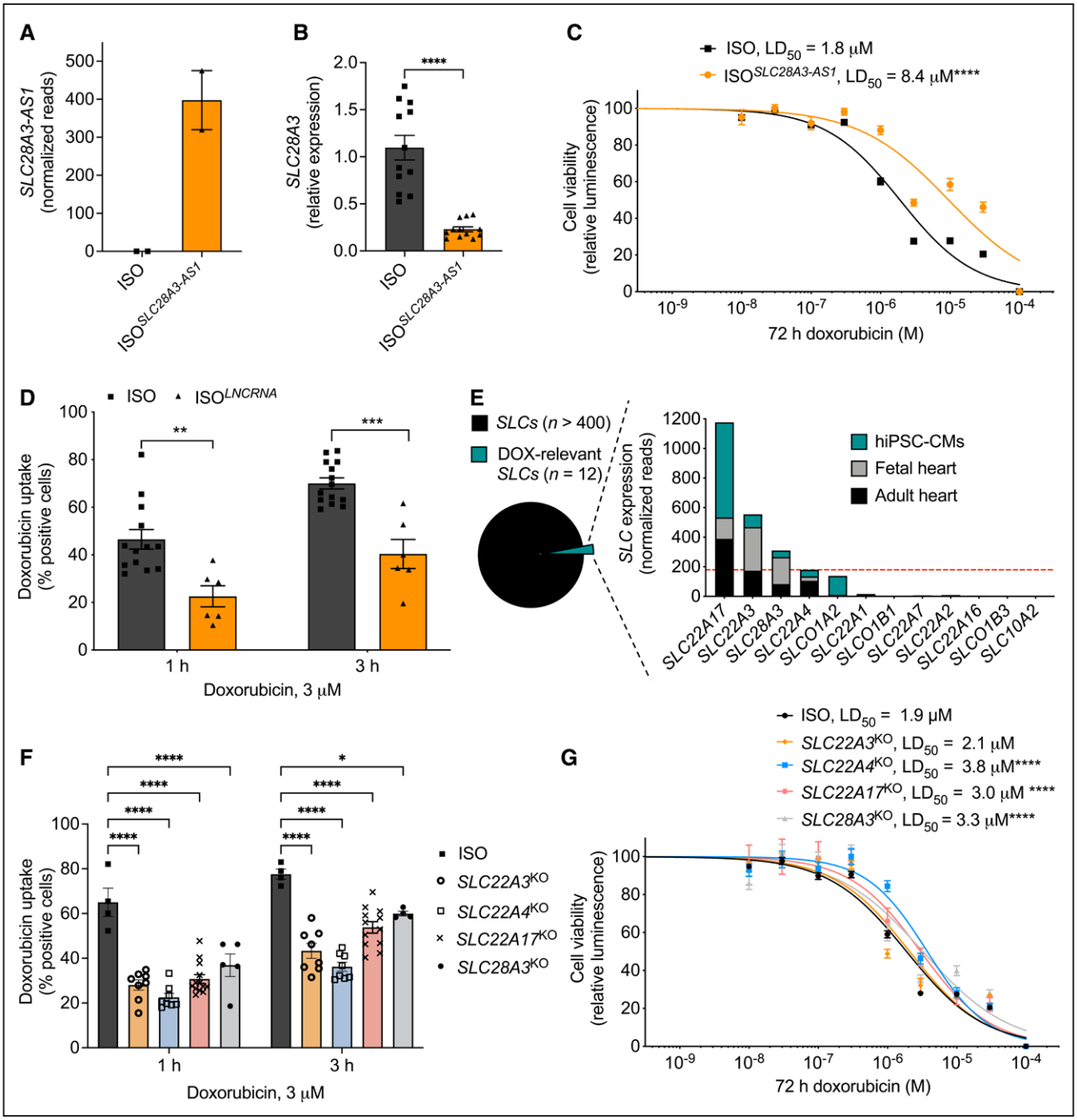

Figure 4. The cardioprotective role of *SLC28A3-AS1*.

A, Relative expression of *SLC28A3-AS1* in ISO hiPSC compared with ISO transduced by viral plasmid encoding *SLC28A3-AS1* cDNA to overexpress *SLC28A3-AS1* ($ISO^{SLC28A3\text{-}AS1}$) assessed by RNA–Seq (n = 2). **B**, *SLC28A3* relative expression in ISO and $ISO^{SLC28A3\text{-}AS1}$ hiPSC-CMs (n = 5–11) assessed by real-time PCR. **C**, Effect of *SLC28A3-AS1* overexpression on cell viability after doxorubicin (72 h) treatment, ISO (n = 17), $ISO^{SLC28A3\text{-}AS1}$ (n = 12). **D**, Effect of *SLC28A3-AS1* overexpression on doxorubicin uptake 1 h and 3 h after doxorubicin treatment (n = 6–14). **E**, Relative human cardiomyocyte expression of SLC transporters (n = 12) previously identified as transporting doxorubicin or a doxorubicin metabolite and/or by genetic associations with doxorubicin clinical outcomes. Red dashed line denoted for the expression cutoff for SLC transporter selection. **F**, Effect of knocking out doxorubicin-relevant SLC transporters on doxorubicin uptake into patient-derived cardiomyocytes [$SLC28A3^{KO}$, $SLC22A4^{KO}$, $SLC22A3^{KO}$, and $SLC22A17^{KO}$ (n = 5–13)]. **G**, Effect of knocking out potential cardiac-specific SLC transporters on cell viability after doxorubicin treatment [$SLC28A3^{KO}$ (n = 14), $SLC22A4^{KO}$ (n = 58), $SLC22A3^{KO}$ (n = 17), and $SLC22A17^{KO}$, (n = 10), ISO (n = 128)]. **C** and **G**, Log-logistic nonlinear regression model was used to estimate the value of the 4 parameters and a t-statistic was used to test for significant difference in LD_{50} between groups. N = full independent experimental replicates. Error bars indicate SEM; $^{*}P \leq 0.05$, $^{**}P \leq 0.01$, $^{***}P \leq 0.001$, $^{****}P \leq 0.0001$ by unpaired 2-tailed Student *t* test (**B**, **D**, and **F**). DOX indicates doxorubicin; hiPSC-CMs, human induced pluripotent stem cell–derived cardiomyocytes; ISO, isotype; SEM, standard error of the mean; SLC, solute carrier; SLC28A3, solute carrier family 28 member 3; and *SLC28A3-AS1*, *SLC28A3* overlapping antisense long noncoding RNA.

(*SLC22A4*^{KO}, *SLC22A3*^{KO}, and *SLC22A17*^{KO}) and differentiated them to cardiomyocytes (Figure S7). We examined the effect of altered expression of each candidate transporter on doxorubicin intracellular uptake and cell viability after doxorubicin treatment. Expectedly, *SLC22A3*, *SLC22A4*, *SLC28A3*, and *SLC22A17* KO resulted in a significant decrease in doxorubicin uptake in isogenic hiPSC-CMs (Figure 4F). DIC quantification revealed that *SLC22A4*^{KO} cardiomyocytes (LD_{50} = 3.8 μmol/L, n = 58; P<0.0001), *SLC28A3*^{KO} cardiomyocytes (LD_{50} = 3.3 μmol/L, n = 17; P<0.0001), and *SLC22A17*^{KO} cardiomyocytes (LD_{50} = 3 μmol/L, n = 10; P=0.005) were less sensitive to doxorubicin and more protected against DIC as compared with ISO (LD_{50} = 1.9 μmol/L, n = 128; P < 0.0001). However, knocking out *SLC22A3* had a detectable but not significant effect on DIC (LD_{50} = 2.1 μmol/L, n = 17; P = 0.5; Figure 4G).

High-Throughput Drug Screening Reveals SLC Inhibitor Desipramine as Novel Cardioprotective Drug Against DIC in hiPSC-CMs and Murine

Because SLC transporters affect DIC and represent well-founded druggable targets, we examined whether SLC substrates can alter doxorubicin uptake and subsequently regulate DIC in hiPSC-CMs. We tested this by first screening 17 drugs with well-established roles in affecting SLC transporter efficacy in relation to doxorubicin uptake (Table S12). To eliminate potential toxicity from high doses of the SLC substrate drugs, LD_{50} was determined in our ISO cardiomyocytes for the 17 drugs to determine relevant maximum tolerable dose (Figure S8). This target-focused screening revealed that desipramine was the only substrate that altered doxorubicin uptake at both 1 hour and 3 hours after doxorubicin treatment. Doxorubicin uptake was significantly lower in cells that were cotreated with desipramine (3 μmol/L) plus doxorubicin (3 μmol/L), as compared with cells treated with doxorubicin (3 μmol/L) only, after 1 hour (P=0.008) and 3 hours (P=0.04) after treatment (Figure S9A and S9B). Because desipramine significantly decreased doxorubicin transport into cardiomyocytes, we next inspected whether lower doxorubicin intracellular concentration in desipramine pretreated cells affect the magnitude of DIC.

Next, we aimed to expand our screening for novel cardioprotectants by testing the cardioprotective role of the Prestwick Chemical Library that includes 1219 drugs. Cells were pretreated with 3 μmol/L of relevant drugs for 24 hours, then cotreated with relevant drug (3 μmol/L) and doxorubicin (10 μmol/L) for 72 hours, after which DIC was quantified. For each plate, untreated and doxorubicin (10 μmol/L) only–treated cells were included to serve as negative and positive controls, respectively. Drug library screening reveled 34 cardioprotective molecules that attenuated cell death after doxorubicin treatment (Figure 5A). Drug repurposing is significantly faster and more cost-effective than de novo drug discovery approaches, and thus we focused on the top US Food and Drug Administration–approved drugs identified from our screening. It is interesting that the top 10 significant cardioprotectants included 6 US Food and Drug Administration–approved drugs (fluoxetine, butoconazole, perospirone, tetracaine, propofol, and desipramine [Figure 5B]); of these drugs, desipramine again showed the most significant protection against doxorubicin-induced cardiomyocyte death (P=0.007; 2.5-fold; Figure 5A–5B). To further validate these results, we then investigated the cardioprotective effect of these US Food and Drug Administration–approved cardioprotective drugs against 10 log-doses of doxorubicin. This analysis showed that desipramine has the strongest cardioprotective effect when compared with cells treated only with doxorubicin (LD_{50} = 10.66 μmol/L; P<0.0001), followed by propofol (LD_{50} = 4.77 μmol/L; P=0.003), then tetracaine (LD_{50} = 4.65 μmol/L; P<0.001), then butoconazole (LD_{50} = 4.4 μmol/L; P=0.01; Figure 5C and 5D; Figure S9C).

On the basis of these findings, we selected desipramine as our lead cardioprotective drug, and thus, we then investigated whether desipramine could attenuate DIC in vivo. For that, we treated mice with doxorubicin (intraperitoneal 3 mg/kg 2× per week for 3 weeks) plus desipramine (20 $mg \cdot kg^{-1} \cdot day^{-1}$ infusion for 3 weeks) or water as a vehicle control. Doxorubicin treatment results in a steady decline in cardiac function, as assessed by fractional shortening. Importantly, cardiac function was significantly less attenuated by doxorubicin at three weeks with desipramine (P<0.05), compared with vehicle treatment (Figure 5E and 5F; Figure S12B and S12C, Table S13). To rule out the possibility that desipramine could diminish the chemotherapeutic effect of doxorubicin, we studied 8 cancer cell lines—representing breast, liver, colorectal, prostate, uterus, cervix, and bone cancers—and found that cotreatment with desipramine did not impede the anticancer efficacy of doxorubicin in any of these lines (Figure 5F; Figure S10).

DISCUSSION

The identification of reliable predictive genomic biomarkers for DIC and the discovery of efficient cardioprotectants are indispensable to enhance the clinical utility of doxorubicin in cancer treatment. The identification of gene variants predictive of altering DIC through GWAS has provided impetus for developing platforms to confirm these GWAS hits, moving them from "association" to "confirmed mechanism." In this work, we demonstrated that the patient-specific hiPSC-CM model is ideal for studying the implication of transporter inhibitors and genetic variants in DIC. We show that patient-specific cardiomyocytes recapitulate the cardioprotective effect of the CGAS-identified *SLC28A3* locus; confirm for the first time the role of *SLC28A3* in DIC independent of patient-specific genetic

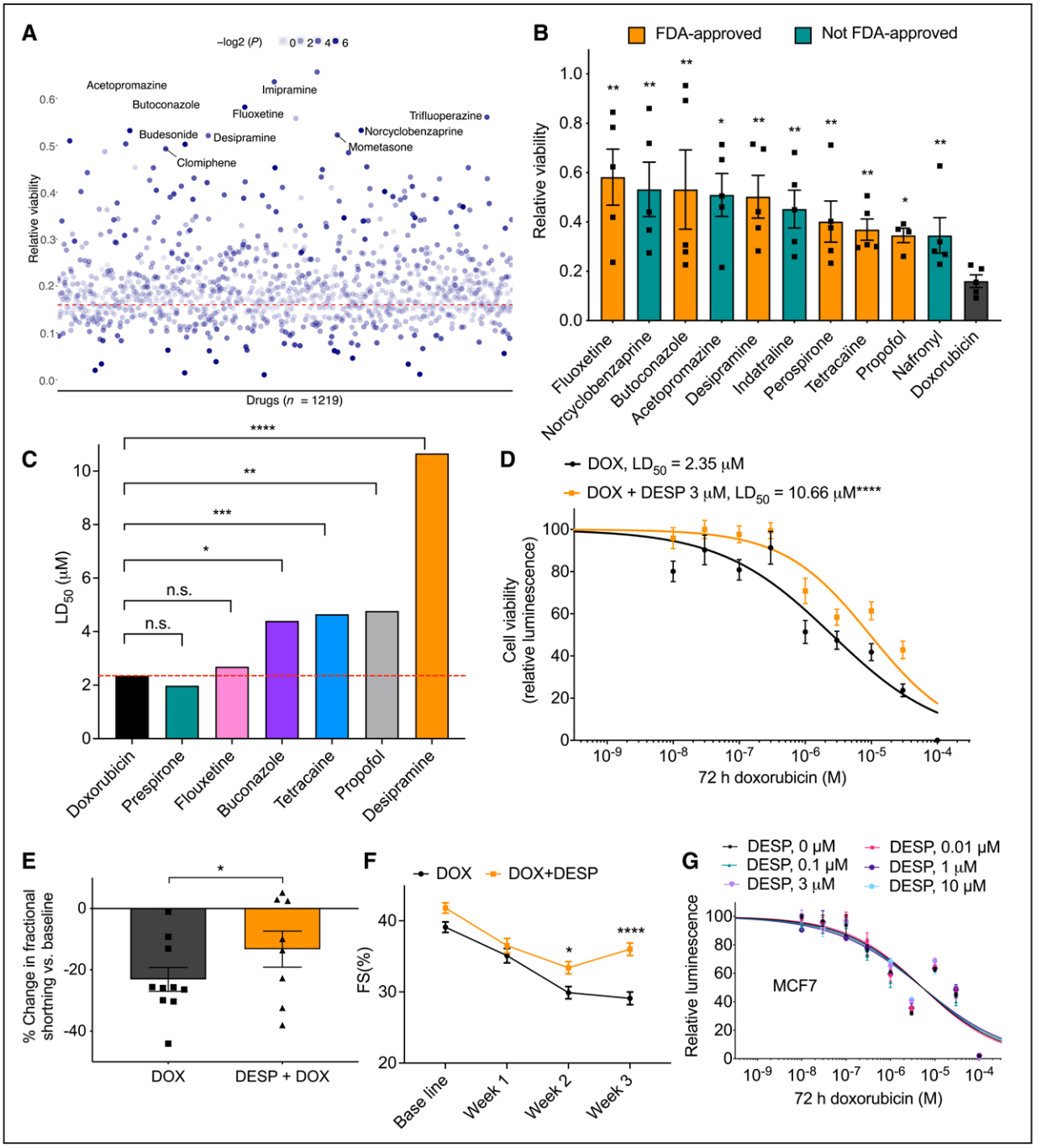

Figure 5. Multimodality drug screening identifies DESP as a novel effective cardioprotectant against DOX-induced cardiotoxicity. **A**, Prestwick Chemical Library screening (n = 1219) in relation to DOX-induced cardiotoxicity (n = 5). All drugs were used at 3 μmol/L. Red dashed line indicates cell viability 72 h after DOX treatment (10 μmol/L); the top 10 significant cardioprotective drugs based on cell viability are labeled. **B**, Bar plot showing top 10 significant cardioprotective drugs (on the basis of *P* value) compared with DOX alone (72 h; 10 μmol/L)–treated cells. Non–FDA-approved drugs are indicated with teal bars. **C**, Further validation of top FDA-approved drugs (identified from the Prestwick Library screening) against 10 log doses of DOX. **D**, Effect of cotreatment of DESP (3 μmol/L) and DOX (72 h) on human induced pluripotent stem cell–derived cardiomyocyte viability (DOX [n = 42]; DOX + DESP [n = 35]). **E**, Percent change in ventricular fraction shortening normalized to baseline, after 3 weeks of DOX treatment (3 mg/kg IP; n = 10) compared cotreatment (n = 8) of DESP (20 $mg \cdot kg^{-1} \cdot d^{-1}$; Alzet pump) and DOX (3 mg/kg IP) in mice. **F**, Ventricular fractional shortening at baseline, 1, 2, and 3 weeks after treatment. **G**, Assessment of cell viability of MCF-7 (Michigan Cancer Foundation 7), a breast cancer cell line, after 72 h of DOX and DESP cotreatment (n = 12–20). **D** and **G**, A log-logistic nonlinear regression model was used to estimate the value of the 4 parameters, and t-statistic was used to test for significant difference in LD_{50} between different groups. *F* = full independent experimental replicates. Error bars indicate SEM; $^{*}P < 0.05$, $^{**}P \le 0.01$, $^{***}P < 0.001$, $^{****}P < 0.0001$ by unpaired 2-tailed Student *t* test (**A**–**C** and **E**) and by ANOVA with post hoc testing (**F**). DESP indicates desipramine; DOX, doxorubicin; FDA, US Food and Drug Administration; and SEM, standard error of the mean.

background; and critically reveal that another SNP within this cardioprotective locus, rs11140490 has the highest likelihood to be causal. Furthermore, this platform allowed us to discover that the SLC competitive inhibitor, desipramine protects against DIC without hampering doxorubicin chemotherapy efficacy.

The *SLC28A3* genetic variant rs7853758 is the most robustly replicated AIC strongly associated cardioprotective loci. We show that rs7853758 is in perfect linkage disequilibrium with 23 other SNPs of which 22 are noncoding variants, forming the cardioprotective Hap^{SLC28A3}. Pinpointing causal SNP within this locus is crucial for clinical translation because testing for the causal variant guarantees the detection of the best possible clinical correlation with AIC. Almost 93% of phenotype-associated genetic variants are noncoding.[27] Using the ENCODE (Encyclopedia of DNA Elements) project dataset, it has been shown that ≈80% of GWAS-identified noncoding SNPs are not the causal SNP.[28] Using our recently developed cost-effective fine-mapping pipeline,[29] we found that rs11140490, but not the CGAS-identified hit rs7853758, is the variant with the highest likelihood to be causal in DIC.

Editing only the rs11140490 cardioprotective genotype (CT) back to the reference genotype (TT) in patient-specific hiPSC-CMs renders these cardiomyocytes more susceptible to DIC confirming the causality of this novel variants. It is interesting that editing rs11140490 increase the sensitivity of hiPSC-CMs by ≈28% which is modest and thus denotes that there might be more SNPs within the Hap^{SLC28A3} that interact in an additive manner with rs11140490 to predispose to protection against DIC

Going forward, we propose that a simple clinical test to detect the presence of rs11140490 can be used to predict that a patient will be less likely to experience DIC and that, with future clinical trials, it may be possible for these patients to be treated with a longer duration (higher cumulative dose) of doxorubicin to enhance the efficacy of their chemotherapy. Similarly, the rs11140490 genetic testing could be used as a part of a polygenic cardiotoxicity risk stratification score for doxorubicin-containing chemotherapy regimens such that the protective effect of rs11140490 could balance out for a risk factor that would have otherwise prevented the administration of a relevant doxorubicin-containing chemotherapy regimen to a particular patient.

SLC28A3 encodes a cardiac-specific uptake transporter that has no or marginal expression in several cancer cells and hence, represents a highly druggable target to screen for cardioprotective agents. A large number of drugs have been identified as being trafficked by *SLC* transporters, which explains the substantial role of these transporters in both drug pharmacokinetics and pharmacodynamics and emphasizes the importance of this class of transporters in drug response disposition.[30] Our high-throughput drug screening discovered that treating patient-specific cardiomyocytes with the *SLC* inhibitor desipramine protects against DIC through decreasing the intracellular uptake of doxorubicin into human heart. Our results suggest that a single dose of 3 μmol/L desipramine 24 hours before the administration of doxorubicin in addition to another dose of 3 μmol/L desipramine coadministered with doxorubicin is sufficient for protecting against DIC.

Desipramine is a tricyclic antidepressant sold under the brand name Norpramin and was first patented in 1962.[31] The typical adult dose of desipramine is 100 mg to 200 mg/day. In more severely ill patients, the dosage may be gradually increased to 300 mg/day if necessary. The typical therapeutic concentration is 100 to 300 ng/mL with daily dosing. Our 3-μmol/L in vitro dose would be 798 ng/mL; it is important to note that our preliminary data suggest that just 2 doses, or potentially 1 dose per cycle, of doxorubicin would be required to attenuate DIC. We would therefore suggest that these desipramine doses are potentially within the acceptable clinical range, although further animal model work to confirming dosing strategy is required before clinical trial.

Desipramine is far from an ideal drug, being the most potent sodium channel blocker among its group and causing cardiotoxicity when used chronically. Desipramine-treated patients have been shown to have significantly lower rates of sinus pauses and junctional rhythm, but significantly higher rates of single or paired premature atrial contractions and runs of supraventricular tachycardia as well as lengthening of the QT interval. The solution to this is to develop a desipramine derivative without the sodium channel blockade effect, although approach eliminates the primary advantage of repurposing a drug like desipramine to attenuate DIC. Still, the advantage of using our hiPSC-CM platform for subsequent testing will be a major advantage in such an effort

The majority (56%) of candidate drugs have failed in clinical trial because of lack of efficacy, most likely because the preclinical models used to test the drug does not recapitulate what happens in humans[32] or in the specific target cell type. Additionally, studies staring with genetic correlations in genes encoding targets increases the success rate in clinical development by 2-fold.[33] Patient-derived hiPSC-CMs provides a unique platform that first permits a thorough validation of GWAS-identified AIC-associated loci, and second recapitulate alteration in DIC phenotype in a human-relevant manner. Hence the utilization of hiPSC-CMs in the development of cardioprotectants substantially improves the potential of developing novel derivatives of desipramine that have the same SLC28A3 competitive inhibition effect as desipramine without the well-known side effects common to the tricyclic antidepressant drug family.

It is clear that hiPSC-CMs do not fully mimic the human whole-body model and do not recapitulate all the steps of drug pharmacokinetics and pharmacodynamics. However, hiPSC-CM generation methodologies of the present have enhanced the robustness, purity, maturation, and scalability

to a point where these cells are suitable for a wide range of disease modeling and drug response assays.[34–42] Here we demonstrated that patient-specific cardiomyocytes recapitulate intraindividual variability in genomic-dependent DIC susceptibility. We show that hiPSC-CMs are appropriate to study drug response–associated loci especially for genes with a known mechanism of action such as transporter-encoding genes. The integration of CRISPR/Cas9–based genetic editing to our patient-specific hiPSC model proves to be a powerful tool in identify causal genetic variations in relation to a specific drug response. The expansion of the utility of patient-specific hiPSC-CMs to study additional anthracycline-relevant loci, as well as those of other anticancer agents, will help to identify patient-/population-specific chemotherapeutic-induced cardiotoxicity genetic biomarkers and new cardioprotective agents. Ultimately, the information derived from this platform may allow physicians to tailor chemotherapeutics doses on the basis of patient genotype, bringing the promise of personalized medicine to the field of cardio-oncology.

ARTICLE INFORMATION

Received May 19, 2021; accepted October 29, 2021.

Affiliations

Department of Pharmacology, and the Center for Pharmacogenomics, Northwestern University Feinberg School of Medicine, Chicago, IL (T.M., M.J., H-H.K., C.J.W., D.L-L., H.F., M.R-T., M.G., H.J., P.W.B.). Division of Cardiology, Department of Pediatrics, Stanford University School of Medicine, Stanford, CA (G.F., D.B.). British Columbia Children's Hospital Research Institute (C.J.D.R., B.C.C.); Faculty of Pharmaceutical Sciences (C.J.D.R.); Division of Translational Therapeutics, Department of Pediatrics (B.C.C.), University of British Columbia; and Pharmaceutical Outcomes Program, British Columbia Children's Hospital (B.C.C.), Vancouver, Canada.

Acknowledgments

P.W.B. and T.M. designed the research for this work. T.M., M.J., H-H.K., C.W., D.L-L., H.F., M.R-T., M.G., H.J., and P.W.B. performed the experiments; G.F. and D.B. designed and the performed mouse experiments; C.J.D.R. and B.C.C determined the anthracycline-induced cardiotoxicity phenotype to be used for patient recruitment and provided patient samples; and P.W.B. supervised the project. T.M. and P.W.B. wrote the final article with input from all other authors.

Sources of Funding

This work was supported by the National Institutes of Health (grant Nos. K99/R00 HL121177, R01 CA220002, and R01 CA261898 (to P.W.B.); R33 HL123655 to D.B., B.C.C.), American Heart Association Transformational Project (award No. 18TPA34230105), the Fondation Leducq (to P.W.B.), Canadian Cancer Society (to C.J.D.R., B.C.C., P.W.B.), and Michael Smith Foundation for Health Research Scholar Award (to C.J.R.). Patients from which human induced pluripotent stem cells were derived were recruited by the Canadian Pharmacogenomics Network for Drug Safety (B.C.C., C.J.D.R.) which has received grant funding from the Canadian Institutes for Health Research, Canadian Institutes for Health Research Drug Safety and Effectiveness Network, Genome Canada, Genome British Columbia, and British Columbia Provincial Health Services Authority.

Disclosures

None.

Supplemental Material

Supplemental Methods
Figures S1–S12
Tables S1–S13
References 43–98

REFERENCES

1. Cardinale D, Colombo A, Bacchiani G, Tedeschi I, Meroni CA, Veglia F, Civelli M, Lamantia G, Colombo N, Curigliano G, et al. Early detection of anthracycline cardiotoxicity and improvement with heart failure therapy. *Circulation.* 2015;131:1981-8. doi: 10.1161/CIRCULATIONAHA.114.013777
2. Swain SM, Whaley FS, Ewer MS. Congestive heart failure in patients treated with doxorubicin: a retrospective analysis of three trials. *Cancer.* 2003;97:2869–2879. doi: 10.1002/cncr.11407
3. Avila MS, Ayub-Ferreira SM, de Barros Wanderley MR Jr, das Dores Cruz F, Gonçalves Brandão SM, Rigaud VOC, Higuchi-Dos-Santos MH, Hajjar LA, Kalil Filho R, et al. Carvedilol for prevention of chemotherapy-related cardiotoxicity: the CECCY trial. *J Am Coll Cardiol.* 2018;71:2281–2290. doi: 10.1016/j.jacc.2018.02.049
4. Magdy T, Burmeister BT, Burridge PW. Validating the pharmacogenomics of chemotherapy-induced cardiotoxicity: what is missing? *Pharmacol Ther.* 2016;168:113–125. doi: 10.1016/j.pharmthera.2016.09.009
5. Aminkeng F, Ross CJD, Rassekh SR, Rieder MJ, Bhavsar AP, Sanatani S, Bernstein D, Hayden MR, Amstutz U, Carleton BC. Pharmacogenomic screening for anthracycline-induced cardiotoxicity in childhood cancer. *Br J Clin Pharmacol.* 2017;83:1143–1145. doi: 10.1111/bcp.13218
6. Tan LL, Lyon AR. Role of biomarkers in prediction of cardiotoxicity during cancer treatment. *Curr Treat Options Cardiovasc Med.* 2018;20:55. doi: 10.1007/s11936-018-0641-z
7. Visscher H, Ross CJ, Rassekh SR, Barhdadi A, Dubé MP, Al-Saloos H, Sandor GS, Caron HN, van Dalen EC, Kremer LC, et al; Canadian Pharmacogenomics Network for Drug Safety Consortium. Pharmacogenomic prediction of anthracycline-induced cardiotoxicity in children. *J Clin Oncol.* 2012;30:1422–1428. doi: 10.1200/JCO.2010.34.3467
8. Visscher H, Ross CJ, Rassekh SR, Sandor GS, Caron HN, van Dalen EC, Kremer LC, van der Pal HJ, Rogers PC, Rieder MJ, et al; CPNDS Consortium. Validation of variants in SLC28A3 and UGT1A6 as genetic markers predictive of anthracycline-induced cardiotoxicity in children. *Pediatr Blood Cancer.* 2013;60:1375–1381. doi: 10.1002/pbc.24505
9. Aminkeng F, Ross CJ, Rassekh SR, Hwang S, Rieder MJ, Bhavsar AP, Smith A, Sanatani S, Gelmon KA, Bernstein D, et al; CPNDS Clinical Practice Recommendations Group. Recommendations for genetic testing to reduce the incidence of anthracycline-induced cardiotoxicity. *Br J Clin Pharmacol.* 2016;82:683–695. doi: 10.1111/bcp.13008
10. Fusaki N, Ban H, Nishiyama A, Saeki K, Hasegawa M. Efficient induction of transgene-free human pluripotent stem cells using a vector based on Sendai virus, an RNA virus that does not integrate into the host genome. *Proc Jpn Acad Ser B Phys Biol Sci.* 2009;85:348–362. doi: 10.2183/pjab.85.348
11. Burridge PW, Matsa E, Shukla P, Lin ZC, Churko JM, Ebert AD, Lan F, Diecke S, Huber B, Mordwinkin NM, et al. Chemically defined generation of human cardiomyocytes. *Nat Methods.* 2014;11:855–860. doi: 10.1038/nmeth.2999
12. Burridge PW, Holmström A, Wu JC. Chemically defined culture and cardiomyocyte differentiation of human pluripotent stem cells. *Curr Protoc Hum Genet.* 2015;87:21.3.1–21.3.15. doi: 10.1002/0471142905.hg2103s87
13. Ran FA, Hsu PD, Wright J, Agarwala V, Scott DA, Zhang F. Genome engineering using the CRISPR-Cas9 system. *Nat Protoc.* 2013;8:2281–2308. doi: 10.1038/nprot.2013.143
14. Oceguera-Yanez F, Kim SI, Matsumoto T, Tan GW, Xiang L, Hatani T, Kondo T, Ikeya M, Yoshida Y, Inoue H, et al. Engineering the AAVS1 locus for consistent and scalable transgene expression in human iPSCs and their differentiated derivatives. *Methods.* 2016;101:43–55. doi: 10.1016/j.ymeth.2015.12.012
15. Dandage R, Després PC, Yachie N, Landry CR. Beditor: a computational workflow for designing libraries of guide RNAs for CRISPR-mediated base editing. *Genetics.* 2019;212:377–385. doi: 10.1534/genetics.119.302089
16. Ritz C, Baty F, Streibig JC, Gerhard D. Dose-response analysis using R. *PloS One.* 2015;10:e0146021. doi: 10.1371/journal.pone.0146021
17. Aminkeng F, Bhavsar AP, Visscher H, Rassekh SR, Li Y, Lee JW, Brunham LR, Caron HN, van Dalen EC, Kremer LC, et al; Canadian Pharmacogenomics Network for Drug Safety Consortium. A coding variant in RARG confers susceptibility to anthracycline-induced cardiotoxicity in childhood cancer. *Nat Genet.* 2015;47:1079–1084. doi: 10.1038/ng.3374
18. Churko JM, Burridge PW, Wu JC. Generation of human iPSCs from human peripheral blood mononuclear cells using non-integrative Sendai virus in chemically defined conditions. *Methods Mol Biol.* 2013;1036:81–88. doi: 10.1007/978-1-62703-511-8_7
19. Diecke S, Lu J, Lee J, Termglinchan V, Kooreman NG, Burridge PW, Ebert AD, Churko JM, Sharma A, Kay MA, et al. Novel codon-optimized mini-

intronic plasmid for efficient, inexpensive, and xeno-free induction of pluripotency. *Sci Rep.* 2015;5:8081. doi: 10.1038/srep08081
20. Burridge PW, Holmström A, Wu JC. Chemically defined culture and cardiomyocyte differentiation of human pluripotent stem cells. *Curr Protoc Hum Genet.* 2015;87:21.3.1–21.3.15. doi: 10.1002/0471142905.hg2103s87
21. Magdy T, Burridge PW. The future role of pharmacogenomics in anticancer agent-induced cardiovascular toxicity. *Pharmacogenomics.* 2018;19:79–82. doi: 10.2217/pgs-2017-0177
22. Loman NJ, Quick J, Simpson JT. A complete bacterial genome assembled de novo using only nanopore sequencing data. *Nat Methods.* 2015;12:733–735. doi: 10.1038/nmeth.3444
23. Kundaje A, Meuleman W, Ernst J, Bilenky M, Yen A, Heravi-Moussavi A, Kheradpour P, Zhang Z, Wang J, Ziller MJ, et al. Integrative analysis of 111 reference human epigenomes. *Nature.* 2015;518:317-30. doi: 10.1038/nature14248
24. Zhou J, Troyanskaya OG. Predicting effects of noncoding variants with deep learning-based sequence model. *Nat Methods.* 2015;12:931–934. Doi: 10.1038/nmeth.3547
25. Weisheit I, Kroeger JA, Malik R, Klimmt J, Crusius D, Dannert A, Dichgans M, Paquet D. Detection of deleterious on-target effects after HDR-mediated CRISPR editing. *Cell Rep.* 2020;31:107689. doi: 10.1016/j.celrep.2020.107689
26. Magdy T, Burmeister BT, Burridge PW. Validating the pharmacogenomics of chemotherapy-induced cardiotoxicity: what is missing? *Pharmacol Ther.* 2016;168:113–125. doi: 10.1016/j.pharmthera.2016.09.009
27. Maurano MT, Humbert R, Rynes E, Thurman RE, Haugen E, Wang H, Reynolds AP, Sandstrom R, Qu H, Brody J, et al. Systematic localization of common disease-associated variation in regulatory DNA. *Science.* 2012;337:1190–1195. doi: 10.1126/science.1222794
28. Schaub MA, Boyle AP, Kundaje A, Batzoglou S, Snyder M. Linking disease associations with regulatory information in the human genome. *Genome Res.* 2012;22:1748–1759. doi: 10.1101/gr.136127.111
29. Magdy T, Kuo HH, Burridge PW. Precise and cost-effective nanopore sequencing for post-GWAS fine-mapping and causal variant identification. *iScience.* 2020;23:100971. doi: 10.1016/j.isci.2020.100971
30. Giacomini KM, Huang SM, Tweedie DJ, Benet LZ, Brouwer KL, Chu X, Dahlin A, Evers R, Fischer V, Hillgren KM, et al. Membrane transporters in drug development. *Nat Rev Drug Discov.* 2010;9:215-36. doi: 10.1038/nrd3028
31. Andersen J, Kristensen AS, Bang-Andersen B, Stromgaard K. Recent advances in the understanding of the interaction of antidepressant drugs with serotonin and norepinephrine transporters. *Chem Commun (Camb).* 2009:3677-92. doi: 10.1039/b903035m
32. Arrowsmith J, Miller P. Trial watch: phase II and phase III attrition rates 2011-2012. *Nat Rev Drug Discov.* 2013;12:569. doi: 10.1038/nrd4090
33. Nelson MR, Tipney H, Painter JL, Shen J, Nicoletti P, Shen Y, Floratos A, Sham PC, Li MJ, Wang J, et al. The support of human genetic evidence for approved drug indications. *Nat Genet.* 2015;47:856–860. doi: 10.1038/ng.3314
34. Itzhaki I, Maizels L, Huber I, Zwi-Dantsis L, Caspi O, Winterstern A, Feldman O, Gepstein A, Arbel G, Hammerman H, et al. Modelling the long QT syndrome with induced pluripotent stem cells. *Nature.* 2011;471:225–229. doi: 10.1038/nature09747
35. Malan D, Zhang M, Stallmeyer B, Müller J, Fleischmann BK, Schulze-Bahr E, Sasse P, Greber B. Human iPS cell model of type 3 long QT syndrome recapitulates drug-based phenotype correction. *Basic Res Cardiol.* 2016;111:14. doi: 10.1007/s00395-016-0530-0
36. Carvajal-Vergara X, Sevilla A, D'Souza SL, Ang YS, Schaniel C, Lee DF, Yang L, Kaplan AD, Adler ED, Rozov R, et al. Patient-specific induced pluripotent stem-cell-derived models of LEOPARD syndrome. *Nature.* 2010;465:808–812. doi: 10.1038/nature09005
37. Yazawa M, Hsueh B, Jia X, Pasca AM, Bernstein JA, Hallmayer J, Dolmetsch RE. Using induced pluripotent stem cells to investigate cardiac phenotypes in Timothy syndrome. *Nature.* 2011;471:230–234. doi: 10.1038/nature09855
38. Kim C, Wong J, Wen J, Wang S, Wang C, Spiering S, Kan NG, Forcales S, Puri PL, Leone TC, et al. Studying arrhythmogenic right ventricular dysplasia with patient-specific iPSCs. *Nature.* 2013;494:105–110. doi: 10.1038/nature11799
39. Sun N, Yazawa M, Liu J, Han L, Sanchez-Freire V, Abilez OJ, Navarrete EG, Hu S, Wang L, Lee A, et al. Patient-specific induced pluripotent stem cells as a model for familial dilated cardiomyopathy. *Sci Transl Med.* 2012;4:130ra47. doi: 10.1126/scitranslmed.3003552
40. Wang G, McCain ML, Yang L, He A, Pasqualini FS, Agarwal A, Yuan H, Jiang D, Zhang D, Zangi L, et al. Modeling the mitochondrial cardiomyopathy of Barth syndrome with induced pluripotent stem cell and heart-on-chip technologies. *Nat Med.* 2014;20:616–623. doi: 10.1038/nm.3545
41. Magdy T, Burridge PW. Unraveling difficult answers: from genotype to phenotype in coronary artery disease. *Cell Stem Cell.* 2019;24:203–205. doi: 10.1016/j.stem.2019.01.008
42. Drawnel FM, Boccardo S, Prummer M, Delobel F, Graff A, Weber M, Gérard R, Badi L, Kam-Thong T, Bu L, et al. Disease modeling and phenotypic drug screening for diabetic cardiomyopathy using human induced pluripotent stem cells. *Cell Rep.* 2014;9:810–821. doi: 10.1016/j.celrep.2014.09.055
43. Chou BK, Gu H, Gao Y, Dowey SN, Wang Y, Shi J, Li Y, Ye Z, Cheng T, Cheng L. A facile method to establish human induced pluripotent stem cells from adult blood cells under feeder-free and xeno-free culture conditions: a clinically compliant approach. *Stem Cells Transl Med.* 2015;4:320–332. doi: 10.5966/sctm.2014-0214
44. Kuo HH, Gao X, DeKeyser JM, Fetterman KA, Pinheiro EA, Weddle CJ, Fonoudi H, Orman MV, Romero-Tejeda M, Jouni M, et al. Negligible-cost and weekend-free chemically defined human iPSC culture. *Stem Cell Reports.* 2020;14:256–270. doi: 10.1016/j.stemcr.2019.12.007
45. Kim D, Paggi JM, Park C, Bennett C, Salzberg SL. Graph-based genome alignment and genotyping with HISAT2 and HISAT-genotype. *Nat Biotechnol.* 2019;37:907–915. doi: 10.1038/s41587-019-0201-4
46. Liao Y, Smyth GK, Shi W. The Subread aligner: fast, accurate and scalable read mapping by seed-and-vote. *Nucleic Acids Res.* 2013;41:e108. doi: 10.1093/nar/gkt214
47. Love MI, Huber W, Anders S. Moderated estimation of fold change and dispersion for RNA-seq data with DESeq2. *Genome Biol.* 2014;15:550. doi: 10.1186/s13059-014-0550-8
48. Schmittgen TD, Livak KJ. Analyzing real-time PCR data by the comparative C(T) method. *Nat Protoc.* 2008;3:1101–1108. doi: 10.1038/nprot.2008.73
49. Wick RR, Judd LM, Gorrie CL, Holt KE. Completing bacterial genome assemblies with multiplex MinION sequencing. *Microb Genom.* 2017;3:e000132. doi: 10.1099/mgen.0.000132
50. De Coster W, D'Hert S, Schultz DT, Cruts M, Van Broeckhoven C. NanoPack: visualizing and processing long-read sequencing data. *Bioinformatics.* 2018;34:2666–2669. doi: 10.1093/bioinformatics/bty149
51. Li H. Minimap2: pairwise alignment for nucleotide sequences. *Bioinformatics.* 2018;34:3094–3100. doi: 10.1093/bioinformatics/bty191
52. Li H, Handsaker B, Wysoker A, Fennell T, Ruan J, Homer N, Marth G, Abecasis G, Durbin R; 1000 Genome Project Data Processing Subgroup. The sequence alignment/map format and SAMtools. *Bioinformatics.* 2009;25:2078–2079. doi: 10.1093/bioinformatics/btp352
53. Ramírez F, Ryan DP, Grüning B, Bhardwaj V, Kilpert F, Richter AS, Heyne S, Dündar F, Manke T. deepTools2: a next generation web server for deep-sequencing data analysis. *Nucleic Acids Res.* 2016;44(W1):W160–W165. doi: 10.1093/nar/gkw257
54. Danecek P, Auton A, Abecasis G, Albers CA, Banks E, DePristo MA, Handsaker RE, Lunter G, Marth GT, Sherry ST, et al; 1000 Genomes Project Analysis Group. The variant call format and VCFtools. *Bioinformatics.* 2011;27:2156–2158. doi: 10.1093/bioinformatics/btr330
55. Cingolani P, Patel VM, Coon M, Nguyen T, Land SJ, Ruden DM, Lu X. Using Drosophila melanogaster as a Model for Genotoxic Chemical Mutational Studies with a New Program, SnpSift. *Front Genet.* 2012;3:35. doi: 10.3389/fgene.2012.00035
56. Narasimhan V, Danecek P, Scally A, Xue Y, Tyler-Smith C, Durbin R. BCFtools/RoH: a hidden Markov model approach for detecting autozygosity from next-generation sequencing data. *Bioinformatics.* 2016;32:1749–1751. doi: 10.1093/bioinformatics/btw044
57. Durinck S, Spellman PT, Birney E, Huber W. Mapping identifiers for the integration of genomic datasets with the R/Bioconductor package biomaRt. *Nat Protoc.* 2009;4:1184–1191. doi: 10.1038/nprot.2009.97
58. Braun D, Kim TD, le Coutre P, Köhrle J, Hershman JM, Schweizer U. Tyrosine kinase inhibitors noncompetitively inhibit MCT8-mediated iodothyronine transport. *J Clin Endocrinol Metab.* 2012;97:E100–E105. doi: 10.1210/jc.2011-1837
59. Damaraju VL, Weber D, Kuzma M, Cass CE, Sawyer MB. Selective inhibition of human equilibrative and concentrative nucleoside transporters by BCR-ABL kinase inhibitors: identification of key hENT1 amino acid residues for interaction with BCR-ABL kinase inhibitors. *J Biol Chem.* 2016;291:18809–18817. doi: 10.1074/jbc.M116.741074
60. Braun D, Schweizer U. Authentic bosutinib inhibits triiodothyronine transport by monocarboxylate transporter 8. *Thyroid.* 2014;24:926–927. doi: 10.1089/thy.2013.0660
61. Yin J, Duan H, Wang J. Impact of substrate-dependent inhibition on renal organic cation transporters hOCT2 and hMATE1/2-K-mediated drug transport

and intracellular accumulation. *J Pharmacol Exp Ther.* 2016;359:401–410. doi: 10.1124/jpet.116.236158
62. Tsuda M, Terada T, Ueba M, Sato T, Masuda S, Katsura T, Inui K. Involvement of human multidrug and toxin extrusion 1 in the drug interaction between cimetidine and metformin in renal epithelial cells. *J Pharmacol Exp Ther.* 2009;329:185–191. doi: 10.1124/jpet.108.147918
63. Shitara Y, Itoh T, Sato H, Li AP, Sugiyama Y. Inhibition of transporter-mediated hepatic uptake as a mechanism for drug-drug interaction between cerivastatin and cyclosporin A. *J Pharmacol Exp Ther.* 2003;304:610–616. doi: 10.1124/jpet.102.041921
64. Shitara Y, Takeuchi K, Nagamatsu Y, Wada S, Sugiyama Y, Horie T. Long-lasting inhibitory effects of cyclosporin A, but not tacrolimus, on OATP1B1- and OATP1B3-mediated uptake. *Drug Metab Pharmacokinet.* 2012;27:368–378. doi: 10.2133/dmpk.dmpk-11-rg-096
65. Craddock AL, Love MW, Daniel RW, Kirby LC, Walters HC, Wong MH, Dawson PA. Expression and transport properties of the human ileal and renal sodium-dependent bile acid transporter. *Am J Physiol.* 1998;274:G157–G169. doi: 10.1152/ajpgi.1998.274.1.G157
66. Schroeder A, Eckhardt U, Stieger B, Tynes R, Schteingart CD, Hofmann AF, Meier PJ, Hagenbuch B. Substrate specificity of the rat liver Na(+)-bile salt cotransporter in Xenopus laevis oocytes and in CHO cells. *Am J Physiol.* 1998;274:G370–G375. doi: 10.1152/ajpgi.1998.274.2.G370
67. Taguchi T, Masuo Y, Kogi T, Nakamichi N, Kato Y. Characterization of long-lasting Oatp inhibition by typical inhibitor cyclosporine A and in vitro-in vivo discrepancy in its drug interaction potential in rats. *J Pharm Sci.* 2016;105:2231–2239. doi: 10.1016/j.xphs.2016.04.025
68. Pahwa S, Alam K, Crowe A, Farasyn T, Neuhoff S, Hatley O, Ding K, Yue W. pretreatment with rifampicin and tyrosine kinase inhibitor dasatinib potentiates the inhibitory effects toward OATP1B1- and OATP1B3-mediated transport. *J Pharm Sci.* 2017;106:2123–2135. doi: 10.1016/j.xphs.2017.03.022
69. Xu Q, Wang C, Meng Q, Liu Q, Sun H, Peng J, Ma X, Kaku T, Liu K. OAT1 and OAT3: targets of drug-drug interaction between entecavir and JBP485. *Eur J Pharm Sci.* 2013;48:650–657. doi: 10.1016/j.ejps.2012.12.024
70. Kouzuki H, Suzuki H, Sugiyama Y. Pharmacokinetic study of the hepatobiliary transport of indomethacin. *Pharm Res.* 2000;17:432–438. doi: 10.1023/a:1007576903935
71. Takeda M, Khamdang S, Narikawa S, Kimura H, Hosoyamada M, Cha SH, Sekine T, Endou H. Characterization of methotrexate transport and its drug interactions with human organic anion transporters. *J Pharmacol Exp Ther.* 2002;302:666–671. doi: 10.1124/jpet.102.034330
72. Hu S, Mathijssen RH, de Bruijn P, Baker SD, Sparreboom A. Inhibition of OATP1B1 by tyrosine kinase inhibitors: in vitro-in vivo correlations. *Br J Cancer.* 2014;110:894–898. doi: 10.1038/bjc.2013.811
73. Taguchi T, Masuo Y, Sakai Y, Kato Y. Short-lasting inhibition of hepatic uptake transporter OATP1B1 by tyrosine kinase inhibitor pazopanib. *Drug Metab Pharmacokinet.* 2019;34:372–379. doi: 10.1016/j.dmpk.2019.08.001
74. Oulianova N, Falk S, Berteloot A. Two-step mechanism of phlorizin binding to the SGLT1 protein in the kidney. *J Membr Biol.* 2001;179:223–242. doi: 10.1007/s002320010049
75. David-Silva A, Esteves JV, Morais MRPT, Freitas HS, Zorn TM, Correa-Giannella ML, Machado UF. Dual SGLT1/SGLT2 inhibitor phlorizin ameliorates non-alcoholic fatty liver disease and hepatic glucose production in type 2 diabetic mice. *Diabetes Metab Syndr Obes.* 2020;13:739–751. doi: 10.2147/DMSO.S242282
76. Urakami Y, Akazawa M, Saito H, Okuda M, Inui K. cDNA cloning, functional characterization, and tissue distribution of an alternatively spliced variant of organic cation transporter hOCT2 predominantly expressed in the human kidney. *J Am Soc Nephrol.* 2002;13:1703–1710. Doi: 10.1097/01.asn.0000019413.78751.46
77. Bednarczyk D, Ekins S, Wikel JH, Wright SH. Influence of molecular structure on substrate binding to the human organic cation transporter, hOCT1. *Mol Pharmacol.* 2003;63:489–498. doi: 10.1124/mol.63.3.489
78. Ohashi R, Tamai I, Yabuuchi H, Nezu JI, Oku A, Sai Y, Shimane M, Tsuji A. Na(+)-dependent carnitine transport by organic cation transporter (OCTN2): its pharmacological and toxicological relevance. *J Pharmacol Exp Ther.* 1999;291:778–784.
79. van Montfoort JE, Müller M, Groothuis GM, Meijer DK, Koepsell H, Meier PJ. Comparison of "type I" and "type II" organic cation transport by organic cation transporters and organic anion-transporting polypeptides. *J Pharmacol Exp Ther.* 2001;298:110–115.
80. Cha SH, Sekine T, Fukushima JI, Kanai Y, Kobayashi Y, Goya T, Endou H. Identification and characterization of human organic anion transporter 3 expressing predominantly in the kidney. *Mol Pharmacol.* 2001;59:1277–1286. doi: 10.1124/mol.59.5.1277
81. Yabuuchi H, Tamai I, Nezu J, Sakamoto K, Oku A, Shimane M, Sai Y, Tsuji A. Novel membrane transporter OCTN1 mediates multispecific, bidirectional, and pH-dependent transport of organic cations. *J Pharmacol Exp Ther.* 1999;289:768–773.
82. Nozawa T, Tamai I, Sai Y, Nezu J, Tsuji A. Contribution of organic anion transporting polypeptide OATP-C to hepatic elimination of the opioid pentapeptide analogue [D-Ala2, D-Leu5]-enkephalin. *J Pharm Pharmacol.* 2003;55:1013–1020. doi: 10.1211/0022357021440
83. Vavricka SR, Van Montfoort J, Ha HR, Meier PJ, Fattinger K. Interactions of rifamycin SV and rifampicin with organic anion uptake systems of human liver. *Hepatology.* 2002;36:164–172. doi: 10.1053/jhep.2002.34133
84. Fattinger K, Cattori V, Hagenbuch B, Meier PJ, Stieger B. Rifamycin SV and rifampicin exhibit differential inhibition of the hepatic rat organic anion transporting polypeptides, Oatp1 and Oatp2. *Hepatology.* 2000;32:82–86. doi: 10.1053/jhep.2000.8539
85. Cui Y, König J, Leier I, Buchholz U, Keppler D. Hepatic uptake of bilirubin and its conjugates by the human organic anion transporter SLC21A6. *J Biol Chem.* 2001;276:9626–9630. doi: 10.1074/jbc.M004968200
86. Sekine T, Cha SH, Tsuda M, Apiwattanakul N, Nakajima N, Kanai Y, Endou H. Identification of multispecific organic anion transporter 2 expressed predominantly in the liver. *FEBS Lett.* 1998;429:179–182. doi: 10.1016/s0014-5793(98)00585-7
87. Hirano M, Maeda K, Shitara Y, Sugiyama Y. Drug-drug interaction between pitavastatin and various drugs via OATP1B1. *Drug Metab Dispos.* 2006;34:1229–1236. doi: 10.1124/dmd.106.009290
88. Minematsu T, Giacomini KM. Interactions of tyrosine kinase inhibitors with organic cation transporters and multidrug and toxic compound extrusion proteins. *Mol Cancer Ther.* 2011;10:531–539. Doi: 10.1158/1535-7163.MCT-10-0731
89. Shen H, Yang Z, Zhao W, Zhang Y, Rodrigues AD. Assessment of vandetanib as an inhibitor of various human renal transporters: inhibition of multidrug and toxin extrusion as a possible mechanism leading to decreased cisplatin and creatinine clearance. *Drug Metab Dispos.* 2013;41:2095–2103. doi: 10.1124/dmd.113.053215
90. Cho SK, Kim CO, Park ES, Chung JY. Verapamil decreases the glucose-lowering effect of metformin in healthy volunteers. *Br J Clin Pharmacol.* 2014;78:1426–1432. doi: 10.1111/bcp.12476
91. Oostendorp RL, van de Steeg E, van der Kruijssen CM, Beijnen JH, Kenworthy KE, Schinkel AH, Schellens JH. Organic anion-transporting polypeptide 1B1 mediates transport of Gimatecan and BNP1350 and can be inhibited by several classic ATP-binding cassette (ABC) B1 and/or ABCG2 inhibitors. *Drug Metab Dispos.* 2009;37:917–923. doi: 10.1124/dmd.108.024901
92. Cvetkovic M, Leake B, Fromm MF, Wilkinson GR, Kim RB. OATP and P-glycoprotein transporters mediate the cellular uptake and excretion of fexofenadine. *Drug Metab Dispos.* 1999;27:866–871.
93. Radchenko M, Symersky J, Nie R, Lu M. Structural basis for the blockade of MATE multidrug efflux pumps. *Nat Commun.* 2015;6:7995. doi: 10.1038/ncomms8995
94. Zhang L, Schaner ME, Giacomini KM. Functional characterization of an organic cation transporter (hOCT1) in a transiently transfected human cell line (HeLa). *J Pharmacol Exp Ther.* 1998;286:354–361.
95. Gorboulev V, Ulzheimer JC, Akhoundova A, Ulzheimer-Teuber I, Karbach U, Quester S, Baumann C, Lang F, Busch AE, Koepsell H. Cloning and characterization of two human polyspecific organic cation transporters. *DNA Cell Biol.* 1997;16:871–881. doi: 10.1089/dna.1997.16.871
96. Wu X, Huang W, Ganapathy ME, Wang H, Kekuda R, Conway SJ, Leibach FH, Ganapathy V. Structure, function, and regional distribution of the organic cation transporter OCT3 in the kidney. *Am J Physiol Renal Physiol.* 2000;279:F449–F458. doi: 10.1152/ajprenal.2000.279.3.F449
97. Wu X, George RL, Huang W, Wang H, Conway SJ, Leibach FH, Ganapathy V. Structural and functional characteristics and tissue distribution pattern of rat OCTN1, an organic cation transporter, cloned from placenta. *Biochim Biophys Acta.* 2000;1466:315–327. doi: 10.1016/s0005-2736(00)00189-9
98. Wu X, Huang W, Prasad PD, Seth P, Rajan DP, Leibach FH, Chen J, Conway SJ, Ganapathy V. Functional characteristics and tissue distribution pattern of organic cation transporter 2 (OCTN2), an organic cation/carnitine transporter. *J Pharmacol Exp Ther.* 1999;290:1482–1492.